

Comparing hypervelocity star populations from the Large Magellanic Cloud and the Milky Way

F. A. Evans^{1*}, T. Marchetti², E. M. Rossi¹, J. F. W. Baggen¹, S. Bloor¹,

¹*Leiden Observatory, Leiden University, PO Box 9513, NL-2300 RA Leiden, The Netherlands*

²*European Southern Observatory, Karl-Schwarzschild-Strasse 2, 85748 Garching bei München, Germany*

Accepted XXX. Received YYY; in original form ZZZ

ABSTRACT

We predict and compare the distributions and properties of hyper-velocity stars (HVSs) ejected from the centres of the Milky Way (MW) and the Large Magellanic Cloud (LMC). In our model, HVSs are ejected at a constant rate – equal in both galaxies – via the Hills mechanism and are propagated in a combined potential, where the LMC orbits the MW on its first infall. By selecting $m > 2 M_{\odot}$ HVSs well-separated from the Magellanic Clouds and Galactic midplane, we identify mock HVSs which would stand out from ordinary stars in the stellar halo in future data releases from the *Gaia* satellite and the Vera C. Rubin Observatory’s Legacy Survey of Space and Time (LSST). We find that in these deep surveys, LMC HVSs will outnumber MW ones by a factor ~ 2.5 , as HVSs can more easily escape from the shallower potential of the LMC. At an assumed HVS ejection rate of 10^{-4} yr^{-1} , HVSs detectable in the final *Gaia* data release and LSST from the LMC (MW) will number 125_{-12}^{+11} (50_{-8}^{+7}) and 140_{-11}^{+10} (42_{-7}^{+6}), respectively. The MW and LMC HVS populations show different kinematics and spatial distributions. While LMC HVSs have more modest total velocities and larger Galactocentric distances clustered around those of the LMC itself, HVSs from the MW show broader distributions, including a prominent high-velocity tail above 500 km s^{-1} that contains at least half of the stars. These predictions are robust against reasonable variation of the Galactic potential and of the LMC central black hole mass.

Key words: Galaxy: centre – Magellanic Clouds – Galaxy: kinematics and dynamics – stars: kinematics and dynamics

1 INTRODUCTION

Hyper-velocity stars (HVSs) are stars moving so fast that they are gravitationally unbound from the Galaxy. The existence of such a population of stars was first proposed by Hills (1988), who theorized that a three-body interaction between a binary system and a massive black hole (MBH) at the centre of the Milky Way could disrupt the binary and eject one companion at $\sim 1000 \text{ km s}^{-1}$. The serendipitous discovery by Brown et al. (2005) of a $3 M_{\odot}$ main sequence star in the outer Galactic halo unbound to the Galaxy by its radial velocity alone ($v_{\text{rad}} \simeq 830 \text{ km s}^{-1}$, see Brown et al. 2014) was touted as the first direct observational evidence in favour of this ‘Hills mechanism’ and of hyper-velocity stars in general. Further detections of unbound HVS candidates followed soon after (Hirsch et al. 2005; Edelmann et al. 2005). To date, several dozen HVS candidates have been discovered via targeted searches in the Galactic halo (e.g. Brown et al. 2006, 2009a, 2012, 2014) or via searches in data releases of ongoing large surveys (e.g. Zhong et al. 2014; Huang et al. 2017; Li et al. 2018; Hattori et al. 2018; Marchetti et al. 2019; Koposov et al.

2020; Marchetti 2021). See Brown (2015) for a review of these objects.

HVSs are intriguing tools to study a variety of astrophysical phenomena – the violent and uncertain physical processes that generate them leave an imprint on their kinematics and properties. As objects born in the GC but located in more observationally accessible regions of the sky, HVSs offer a ‘back door’ into investigating the heavily dust-obscured and source-crowded GC environment (see Zhang et al. 2013; Madigan et al. 2014; Rossi et al. 2017), e.g. the nature of the nuclear star cluster (see Böker 2010, for a review) and the growth of Sgr A* and its impact on its environment (Genzel et al. 2010; Bromley et al. 2012). The deceleration and deflection of HVSs during their flights from the GC to the outer halo make them promising dynamical tracers, providing constraints on the shape, size and mass of the Galactic dark matter halo (e.g., Gnedin et al. 2005; Yu & Madau 2007; Kenyon et al. 2008, 2014; Contigiani et al. 2019).

It is worth noting that for most candidate HVSs, existing astrometry is not precise enough to indisputably associate them with an origin in the Galactic Centre (GC)¹. However, especially given the high-precision astrometry provided by the European Space Agency’s *Gaia* mission (Gaia Collabo-

* E-mail: evans@strw.leidenuniv.nl

ration et al. 2016b, 2018, 2021), the GC can be confidently excluded as the birthplace of many HVS candidates (see e.g. Irrgang et al. 2018; Kreuzer et al. 2020). The past trajectories of some candidates seem to point towards the Galactic disc (e.g., Heber et al. 2008; Silva & Napiwotzki 2011; Palladino et al. 2014; Irrgang et al. 2018, 2019; Marchetti et al. 2018). For these disc-ejected main sequence ‘hyper-runaway’ stars, it is currently unclear which physical mechanism(s) are responsible for ejecting them (see discussion in Evans et al. 2020). Often-blamed mechanisms include dynamical encounters in dense systems (Poveda et al. 1967; Leonard & Duncan 1990; Leonard 1991; Perets & Šubr 2012; Oh & Kroupa 2016) and the disruption of a tight binary following a core-collapse event (Blaauw 1961; Tauris & Takens 1998; Portegies Zwart 2000; Tauris 2015; Renzo et al. 2019; Evans et al. 2020).

The kinematics and/or ages of other HVS candidates do not suggest an origin in the inner Milky Way at all. They either have past trajectories pointing away from the Galaxy entirely (see Marchetti et al. 2019) and/or have stellar lifetimes too short to accommodate a journey from the inner Milky Way to their current position. The latter is the case for HVS3 (Edelmann et al. 2005), an $8 M_{\odot}$ HVS candidate at a distance of 61 kpc. Using *Gaia* Data Release 2 astrometry, Erkal et al. (2019a) found its flight time to Galactic pericentre to be ~ 66 Myr, in tension with its nominal main sequence lifetime of only ~ 35 Myr. It was noted as far back as Edelmann et al. (2005), however, that HVS3 is situated only 16.3° from the Large Magellanic Cloud (LMC). An LMC origin for HVS3 was further suggested by Gualandris & Portegies Zwart (2007), who simulate ejections via the Hills mechanism of HVS3-like stars from the LMC, and by Przybilla et al. (2008), who find elemental abundances in HVS3 more similar to reference stars in the LMC than to reference stars in the GC. Indeed, Erkal et al. (2019a) find that the past trajectory of HVS3 tracks directly to the LMC centre and requires a flight time of only ~ 21 Myr. This, along with its putative ejection velocity of ~ 870 km s $^{-1}$ relative to the LMC centre at its point of closest approach, strongly support a Hills mechanism ejection of HVS3, requiring an LMC MBH mass of at least $10^{3.6} - 10^4 M_{\odot}$.

With the confirmation of HVS3 as an HVS of Magellanic origin, it is natural to wonder how many other LMC-ejected HVSs are out there. In light of the ever-increasing population of HVS candidates, it is important to characterize the contribution of the LMC to this population. While the rate at which HVSs are ejected from the LMC centre is currently unconstrained, the LMC remains arguably the most promising extra-Galactic source of HVSs. It is the nearest galaxy massive enough to host an MBH, and its large orbital velocity in the Galactocentric rest frame (~ 320 km s $^{-1}$; Kallivayalil et al. 2013) and modest escape velocity (~ 100 km s $^{-1}$ from the centre to 2 kpc in our default MW+LMC potential) mean that its ejected stars can quite easily escape the inner LMC. Other possible extra-Galactic provenances of HVSs include HVSs ejected from M31 or its satellites (Lu et al. 2007; Sherwin et al. 2008), or HVSs tidally stripped from infalling dwarf galaxies (Abadi et al. 2009).

¹ The notable exception to this is the HVS candidate S5-HVS1 (Koposov et al. 2020), whose short flight time and precise astrometry allow it to be traced back definitively to the GC.

To date, HVS3 remains the only HVS conclusively associated with the LMC. This may change, however, with the advent of massive Galactic surveys targeting billions of Milky Way sources such as the *Gaia* mission and the Vera C. Rubin Observatory’s Legacy Survey of Space and Time (LSST; see Ivezić et al. 2019). In this work we realistically simulate the ejection of HVSs from MBHs located in both the LMC centre and the GC. We propagate these ejected HVSs through a Galactic potential consisting of the Milky Way and a moving LMC. Making reasonable assumptions about the *Gaia* and LSST selection functions, we predict the size and properties of the GC HVS and LMC HVS populations in future data releases from these surveys. By identifying contrasts between the two populations, we provide insight on how LMC HVSs can be most efficiently unearthed. We additionally explore how these predictions depend on the MW+LMC potential and the LMC MBH mass.

This work follows and complements earlier research into the ejection of HVSs from the LMC. Our method of ejecting and propagating stars from the LMC resembles broadly Boubert & Evans (2016), who eject $3 M_{\odot}$ HVSs via the Hills mechanism from the LMC centre to explore their sky distribution on the sky, agnostic of the HVS ejection rate. They predict a dipolar distribution of LMC HVSs – a cluster near the present day LMC location and a corresponding dearth of LMC HVSs in the Galactic northeast. Extending their work, we employ a more comprehensive ejection model and exploit mock *Gaia* and LSST observations to make quantitative predictions on the number of detectable LMC HVSs under an assumed ejection rate. Exploring the possibility that HVSs are ejected from the LMC disc following binary supernovae, Boubert et al. (2017) find that this mechanism can contribute to the known population of Galactic HVS candidates at a rate of $\sim 3 \times 10^{-6}$ yr $^{-1}$, many of which will be observable by *Gaia* (see also Sec. 6.5).

In Sec. 2 we describe our HVS ejection model, our parametrization of MW+LMC potential, our orbital integration, our approach to obtaining mock photometric observations of our sample, and the *Gaia* and LSST selection cuts we employ. In Secs. 3, 4 and 5 we present our results and discuss these results in Sec. 6. We present our conclusions in Sec. 7. To clarify the terminology used in this work, we use for simplicity the term HVS to refer to *any and all* stars ejected from the GC or LMC centre via interactions with an MBH, regardless of ejection velocity. This is a more general use of the term than the convention, which typically refers exclusively to stars unbound to the Milky Way ejected from the GC (e.g. Brown 2015).

2 MOCK EJECTED STAR CATALOGUES

The generation of realistic mock populations of GC and LMC HVSs requires a number of ingredients. In the following subsections we outline how we draw stellar velocities and masses at the moment of ejection, how we assign ages and flight times to ejected stars, how we propagate ejected stars forward in time, and how we obtain mock photometric and astrometric observations for these populations. If not otherwise stated, the methodology is the same for both GC and LMC HVSs.

2.1 Ejection distribution and rate

We generate populations of Hills mechanism-ejected stars from GC and the LMC centre following a Monte Carlo ejection model similar to that outlined in Rossi et al. (2017), Marchetti et al. (2017) and implemented in Marchetti et al. (2018). We describe the model as follows.

We generate binary systems defined by the mass of the primary m_p , the mass ratio between the secondary and primary q and the orbital semi-major axis a . Following an interaction with the MBH, the binary is disrupted – one member star is ejected while the other remains bound to the MBH. Sari et al. (2010) and Kobayashi et al. (2012) show that for a parabolic approach, there is an equal probability for ejecting either star in the binary. We therefore randomly designate one star among the pair as the ejected star. Its ejection velocity is calculated analytically (Sari et al. 2010; Kobayashi et al. 2012; Rossi et al. 2014):

$$v_{\text{ej}} = \sqrt{\frac{2Gm_c}{a}} \left(\frac{M_{\text{BH}}}{M} \right)^{1/6}, \quad (1)$$

where $M = (1 + q)m_p$ is the total mass of the progenitor binary, m_c is the mass of the remaining bound companion, and M_{BH} is the MBH mass. For stars ejected from the GC, we take $M_{\text{BH,GC}} = 4 \times 10^6 M_\odot$ (Eisenhauer et al. 2005; Ghez et al. 2008). For ejections from the LMC centre, we assume in our fiducial model an LMC MBH mass of $10^5 M_\odot$, similar to the median MBH mass quoted by Reines et al. (2013), who study dwarf galaxies with stellar masses similar to the LMC ($10^{8.5} \lesssim M_* \lesssim 10^{9.5} M_\odot$). We explore in Sec. 6 the sensitivity of our results to variation in $M_{\text{BH,LMC}}$.

We draw primary masses for the binaries assuming a Kroupa (2001) mass function in the range $[0.1, 100] M_\odot$, consistent with observations of the central regions of the Milky Way (Bartko et al. 2010; Löckmann et al. 2010) and broadly consistent with observations of LMC clusters at least in the $m > 0.5 M_\odot$ regime (Da Rio et al. 2009; Liu et al. 2009a,b). Mass ratios are sampled in the interval $0.1 \leq q \leq 1$ distributed as $f(q) \propto q^{-3.5}$ and semi-major axes follow Öpik’s law, $f(a) \propto a^{-1}$ (Öpik 1924), both consistent with Dunstall et al. (2015) who investigate B-type binaries in the VLT-FLAMES Tarantula Survey of the 30 Doradus region in the LMC (Evans et al. 2011). Modest variations in the power law indices for the distributions described above, including switching to a more top-heavy GC initial mass function (IMF) as suggested by Lu et al. (2013), do not significantly impact the results of this study. Binary orbital semi-major axes are generated in the range $2.5 \max(R_p, R_s) \leq a \leq 2000 R_\odot$, where R_p and R_s are the stellar radii of the primary and secondary stars, respectively. This lower limit is set by Roche lobe overflow. Finally, we remove stars less massive than $0.5 M_\odot$, as these ejected stars will more than likely be too faint for current or near-future surveys to detect.

We show in Fig. 1 the distributions of ejection velocities resulting from Eq. 1 and the above assumptions for HVS ejections from both the GC and LMC. The median HVS ejection velocity from the GC is 370 km s^{-1} . Note that in our MW+LMC potential (see Sec. 2.3), the escape velocity from the GC to 2 kpc is $\sim 600 \text{ km s}^{-1}$ – only 36 per cent of stars are ejected with sufficient velocity to escape the Galactic bulge. The median ejection velocity from the LMC centre is 200 km s^{-1} in the LMC rest frame. Despite lower typical ejection

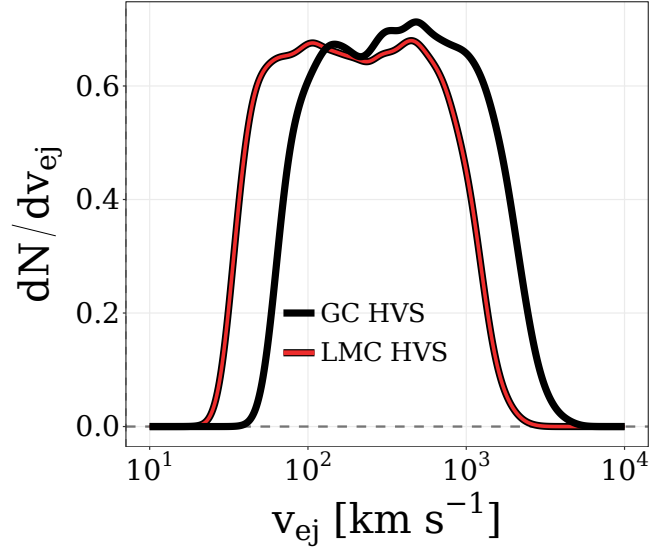


Figure 1. Distribution of stellar ejection velocities via the Hills mechanism (see Sec. 2.1) in the rest frame of the MBH in the LMC centre (red; $M_{\text{BH,LMC}} = 1 \times 10^5 M_\odot$) and GC (black; $M_{\text{BH,GC}} = 4 \times 10^6 M_\odot$).

tion velocities, ~ 70 per cent of stars ejected from the LMC centre will escape the inner LMC owing to its modest effective escape velocity (100 km s^{-1} to 2 kpc in our MW+LMC potential).

Generated HVSs are ejected isotropically on initially radial trajectories in the Galactocentric and LMC-centric rest frames for the GC and LMC HVS populations, respectively. For LMC ejections we assume the LMC MBH is coincident with our assumed LMC centre at $\alpha = 78.76^\circ$, $\delta = -69.19^\circ$ (Zivick et al. 2019). In at least a substantial fraction of dwarf galaxies, the MBH can be offset by the host dwarf centre by as much as a few kiloparsecs (see Reines et al. 2020; Mezcua & Domínguez Sánchez 2020; Bellovary et al. 2021). A modest deviation of the LMC MBH in position and velocity from the assumed LMC centre does not appreciably affect our predictions for the number of GC and LMC HVSs lurking in future surveys.

Theoretical estimates and observational constraints imply an HVS ejection rate from the GC of $\sim 10^{-5} - 10^{-3} \text{ yr}^{-1}$ (see Brown 2015). We adopt a constant ejection rate of 10^{-4} yr^{-1} from the GC in all models. In light of the lack of observational constraints on the putative LMC MBH and its stellar environment, we assume the HVS ejection rate from the LMC centre to be 10^{-4} yr^{-1} as well. We discuss further the uncertainty surrounding the HVS ejection rate in Sec. 6.2. Our characterization of the spatial distribution and kinematics of HVS candidates observable by these surveys will be stacked and averaged over multiple ejection samples, and will thus not depend on the ejection rate.

2.2 HVS flight time distribution

In addition to masses and initial velocities, we assign each ejected star a flight time and a stellar age at ejection. For HVS ejections from the GC we consider ejections throughout the entire lifetime of the Milky Way, assumed here to have

formed shortly after the Big Bang 13.8 Gyr ago (Planck Collaboration et al. 2016). The LMC is most likely on its first infall, having first crossed the virial radius some $\sim 1.5\text{--}4$ Gyr ago (Besla et al. 2007; Kallivayalil et al. 2013; Gómez et al. 2015; Patel et al. 2017). We therefore consider ejections from the LMC over the last 4 Gyr².

Our present day mock catalogue of HVSs is composed of stars ejected t_{ej} ago that have not yet left the main sequence. We assign t_{ej} uniformly:

$$t_{\text{ej}} = \epsilon_1 \cdot 4 \text{ Gyr} \quad \text{from LMC} \quad (2)$$

$$t_{\text{ej}} = \epsilon_1 \cdot 13.8 \text{ Gyr} \quad \text{from GC}, \quad (3)$$

where $0 < \epsilon_1 < 1$ is a uniform random number. We assume no preferred stellar age at time of ejection. The age of a star at ejection $t_{\text{age,ej}}$ is then a random fraction ϵ_2 of its main sequence lifetime t_{MS} :

$$t_{\text{age,ej}} = \epsilon_2 \cdot t_{\text{MS}}, \quad (4)$$

where t_{MS} is calculated according to the stellar mass and assumed metallicity using the Hurley et al. (2000) analytical formulae. Though stars in the GC show a large spread in metallicity (Do et al. 2015; Feldmeier-Krause et al. 2017; Rich et al. 2017), for GC HVSs we assume solar metallicity, $Z_{\odot} = 0.02$ (Anders & Grevesse 1989). For the LMC HVSs we assume a lower metallicity of $\log_{10}[Z/Z_{\odot}] = -0.5$ (see Moe & Stefano 2013; Piatti & Geisler 2013; Choudhury et al. 2016, and references therein).

The remaining main sequence lifetime of the star t_{left} is

$$t_{\text{left}} = t_{\text{MS}} - t_{\text{age,ej}} = (1 - \epsilon_2) \cdot t_{\text{MS}}. \quad (5)$$

We restrict our analysis to main sequence stars to more easily compare with existing HVS candidates. We therefore remove stars for whom $t_{\text{ej}} > t_{\text{left}}$. The flight time of each mock HVS is then

$$t_{\text{flight}} = t_{\text{ej}} \quad (6)$$

and its current age is

$$t_{\text{age,0}} = t_{\text{age,ej}} + t_{\text{flight}}. \quad (7)$$

These stellar ages are useful in obtaining mock photometry (see Sec. 2.5).

After assigning masses, ejection velocities, flight times and ages to each HVS according to Eqs. 1-7, removing $m < 0.5 M_{\odot}$ stars and stars which don't survive on the main sequence until the present day, we are left with samples of $\sim 70,000$ GC HVSs and $\sim 37,000$ LMC HVSs. We draw, eject and propagate 50 HVS samples from each origin to eliminate stochastic effects on our predictions.

2.3 Milky Way + LMC potential

We describe here the MW + moving LMC potential through which we propagate our ejected HVS. We explore variations

² The precise lookback time up to which we consider LMC HVS ejections is not particularly important when predicting HVS populations in *Gaia* or LSST – stars with flight times > 1 Gyr are generally too far (and thus too dim) to be detectable by these surveys (see Sec. 4)

in these assumptions in Sec. 6. We model the MBH in the Galactic Centre by a Keplerian potential,

$$\Phi_{\text{BH,GC}}(r) = -G \frac{4 \times 10^6 M_{\odot}}{r}, \quad (8)$$

where r is the Galactocentric distance. The Galactic bulge is treated as a Hernquist potential (Hernquist 1990),

$$\Phi(r) = -\frac{GM_{\text{b}}}{r + r_{\text{b}}}, \quad (9)$$

where $M_{\text{b}} = 3.4 \times 10^{10} M_{\odot}$ and $r_{\text{b}} = 0.7 \text{ kpc}$ are the bulge scale mass and radius, respectively (Price-Whelan et al. 2014). For the Galactic disc we use a Miyamoto-Nagai potential in Galactocentric cylindrical coordinates, (Miyamoto & Nagai 1975),

$$\Phi(R, z) = -\frac{GM_{\text{d}}}{\sqrt{R^2 + (a_{\text{d}} + \sqrt{z^2 + b_{\text{d}}^2})}}, \quad (10)$$

where M_{d} is the disc mass and a_{d} and b_{d} are the disc scale length and height, respectively. We use $M_{\text{d}} = 10^{11} M_{\odot}$, $a_{\text{d}} = 6.5 \text{ kpc}$ and $b_{\text{d}} = 260 \text{ pc}$ following Price-Whelan et al. (2014).

We model the contribution from Milky Way dark matter halo using a spheroidal NFW potential (Navarro et al. 1996, 1997):

$$\rho(x, y, z) = \frac{M_{\text{s}}}{4\pi r_{\text{s}} (\xi/r_{\text{s}})(1 + \xi/r_{\text{s}})^2}, \quad \xi^2 = x^2 + y^2 + \frac{z^2}{c_{\text{halo}}}, \quad (11)$$

where M_{s} and r_{s} are the scale mass and radius of the halo, respectively, and c_{halo} is the dimensionless z-to-x axis ratio of the spheroid. In our fiducial potential we assume $c_{\text{halo}} = 1$ and choose $M_{\text{s}} = 0.76 \times 10^{12} M_{\odot}$ and $r_{\text{s}} = 24.8 \text{ kpc}$ – the best fit parameters to the Galactic rotation curve for a spherical halo from Rossi et al. (2017).

We model the LMC potential as a two-component Keplerian MBH + Hernquist bulge. We assume an LMC MBH mass of $10^5 M_{\odot}$ (see Sec. 2.1). As a fiducial LMC scale mass we choose $M_{\text{LMC}} = 1.5 \times 10^{11} M_{\odot}$ and a corresponding scale radius of $R_{\text{LMC}} = 17.14 \text{ kpc}$. This is a common choice for M_{LMC} (e.g. Erkal et al. 2019a; Belokurov et al. 2019; Erkal et al. 2020), consistent with recent determinations (Kallivayalil et al. 2013; Peñarrubia et al. 2016; Laporte et al. 2018; Erkal et al. 2019b; Erkal & Belokurov 2020). In each simulation, the LMC is initialized at its observed position and velocity today. We use a centre-of-mass position of $\alpha = 78.76^{\circ}$, $\delta = -69.19^{\circ}$ (Zivick et al. 2019), proper motions of $(\mu_{\alpha^*}, \mu_{\delta}) = (1.91, 0.229) \text{ mas yr}^{-1}$ (Kallivayalil et al. 2013), heliocentric distance of 49.97 kpc (Pietrzyński et al. 2013) and radial velocity of $+262.2 \text{ km s}^{-1}$ (van der Marel et al. 2002).

2.4 Orbital Integration

In both GC and LMC centre ejections, stars are initialized at a random point on the surface of the MBH's so-called 'sphere of influence', where the contribution of the MBH to the total potential becomes subdominant. For the GC MBH we adopt a sphere of influence radius of 3 pc (Genzel et al. 2010). In the absence of constraints on the size of the sphere of influence of the LMC MBH, we adopt this same value. The results of this study are not sensitive to modest variations of this radius.

For each GC HVS and LMC HVS, the LMC is first integrated backwards in time to the star's flight time t_{flight} ago. Stars ejected from the GC are initialized with velocities pointing directly away from the GC. Similarly, LMC-ejected stars are initially placed 3 pc from the LMC centre at the appropriate time and their initial velocities in the Galactocentric rest frame are the vector addition of their ejection velocities in the LMC rest frame and the LMC orbital velocity t_{flight} ago. The LMC and the HVS are both propagated forward in time until the present day. Orbits are integrated in the PYTHON package GALPY³ (Bovy 2015) using a fifth-order Dormand-Prince integrator (Dormand & Prince 1980) with a fixed timestep of 0.1 Myr. We assume the Sun is 8.178 kpc from the GC (The GRAVITY Collaboration et al. 2019) and 25 pc above the Galactic disc (Bland-Hawthorn & Gerhard 2016). We assume a circular velocity at the Solar position of 232.76 km s⁻¹ (McMillan 2017) and take $(U_{\odot}, V_{\odot}, W_{\odot}) = (14.0, 12.24, 7.25)$ km s⁻¹ (Schönrich 2012). The impact of dynamical friction on the LMC's orbit is accounted for using the implementation in GALPY which follows roughly Petts et al. (2016).

2.5 Mock photometric & astrometric observations

After propagating our populations of mock HVSs, we compute photometric properties following Marchetti et al. (2018). Given the mass, metallicity and age of the star today, we obtain its physical radius, effective temperature and surface gravity using the analytic formulae of Hurley et al. (2000). Via chi-squared minimization of the effective temperature and surface gravity, we find the best-fitting stellar spectrum among the $\log_{10}[Z/Z_{\odot}] = 0.0$ spectra (for GC HVSs) or the $\log_{10}[Z/Z_{\odot}] = -0.5$ spectra (for LMC HVSs) in the BaSeL SED Library 3.1 (Westera et al. 2002). We assume an atmospheric micro-turbulence velocity of 2 km s⁻¹ and a mixing length of zero. We calculate the visual extinction A_V at each star's position using the MWDUST⁴ three-dimensional Galactic dust map (Bovy et al. 2016); itself a combination of the Drimmel et al. (2003), Marshall et al. (2006), and Green et al. (2015) maps. The attenuation at all wavelengths A_{λ} is calculated from the visual extinction assuming a Cardelli et al. (1989) reddening law with $R_V = 3.1$. We compute each star's magnitude in the *Gaia* G filter by integrating the flux of the best-fitting BaSeL spectrum and the attenuation A_{λ} through the *Gaia* Early Data Release 3 (EDR3) G passband⁵ (see Jordi et al. 2010, eq. 1). We similarly compute magnitudes in the Johnson-Cousins I_C and V bands, adopting the Bessell (1990) passbands curves. From these, the magnitude in the *Gaia* G_{RVS} band can be computed using the polynomial fits in Jordi et al. (2010). We similarly compute magnitudes in the LSST r band using the expected throughput of the LSST r passband⁶. We use the PYTHON package PyGaia⁷ to estimate the end-of-mission *Gaia* parallax and proper motion uncertainties for each HVS.

³ <https://github.com/jobovy/galpy>

⁴ <https://github.com/jobovy/mwdust>

⁵ <https://www.cosmos.esa.int/web/gaia/edr3-passbands>

⁶ <https://github.com/lsst/throughputs>

⁷ <https://github.com/agabrown/PyGaia>

3 HVS SPACE AND VELOCITY DISTRIBUTIONS

In this Section we explore the space and velocity distributions of all HVSs ejected from the GC and LMC, regardless of they are detectable by *Gaia* or LSST.

In Fig. 2 we show the spatial distribution of GC HVSs and LMC HVSs on the sky. While no region of the sky is entirely inaccessible by LMC HVSs (lower panel), the vast majority of stars are in close proximity to the LMC. A notable feature is the arm of HVSs that leads the LMC orbit. The origin of this arm is the fact that stars ejected from the LMC along its direction of motion will be boosted by its $v_{\text{GC}} \simeq 320$ km s⁻¹ orbital velocity in the MW rest frame (Kallivayalil et al. 2013), reaching higher Galactocentric velocities than stars ejected on angles misaligned with the LMC's orbital motion. These cluster and arm features are consistent with the findings of Boubert & Evans (2016), who suggest the leading arm of LMC HVSs as a possible explanation for the apparent excess of known HVS candidates in the vicinity of Leo (see Brown et al. 2009b). There is also a tail of HVSs lagging the LMC orbit on the sky, though we caution this tail consists mainly of very distant, long- t_{flight} stars which will not be observable by *Gaia* or LSST (see following Section).

Fig. 2 suggests that the vast majority of HVSs ejected from the GC (upper panel) will be in close proximity to the GC on the sky and otherwise mostly confined to the Galactic mid-plane. Due to the large escape velocity from the inner Galaxy, only the HVSs with large ejection velocities will escape the bulge. Only 2.6 per cent of GC HVSs are found today within 25° of the LMC centre. The stark differences between the spatial distributions of GC HVSs and LMC HVSs lend optimism to the prospect of distinguishing the two populations.

In Fig. 3 we show the distribution of HVS velocities and distances in the Galactocentric rest frame after each star has been propagated through the MW+LMC potential. GC-ejected stars with large ejection velocities escape the Galaxy and end up today ~thousands of kpc away with Galactocentric velocities not much lower than their ejection velocities. Stars with lower ejection velocities, however, are confined to the inner few kiloparsecs of the Galaxy with significantly lower velocities. LMC HVSs show comparatively tighter distributions in Galactocentric distance and velocity, concentrated near to and slightly farther/faster than the LMC's orbital velocity (320 km s⁻¹) and distance (49 kpc). The median rest frame Galactocentric velocity for LMC HVSs is actually higher than the median ejection velocity in the LMC rest frame. Two factors contribute to this increase – the significant orbital velocity of the LMC in the Galactocentric rest frame and the acceleration of stars ejected towards the MW as they fall deeper into the MW potential well.

4 HYPER-VELOCITY STARS OBSERVABLE BY FUTURE SURVEYS

In the previous Section we explored the properties of *all* surviving HVSs ejected from the GC and LMC centre. Here we select and describe stars both bright enough to be visible by *Gaia* and/or LSST, and conspicuous enough to be recognized as promising HVS candidates.

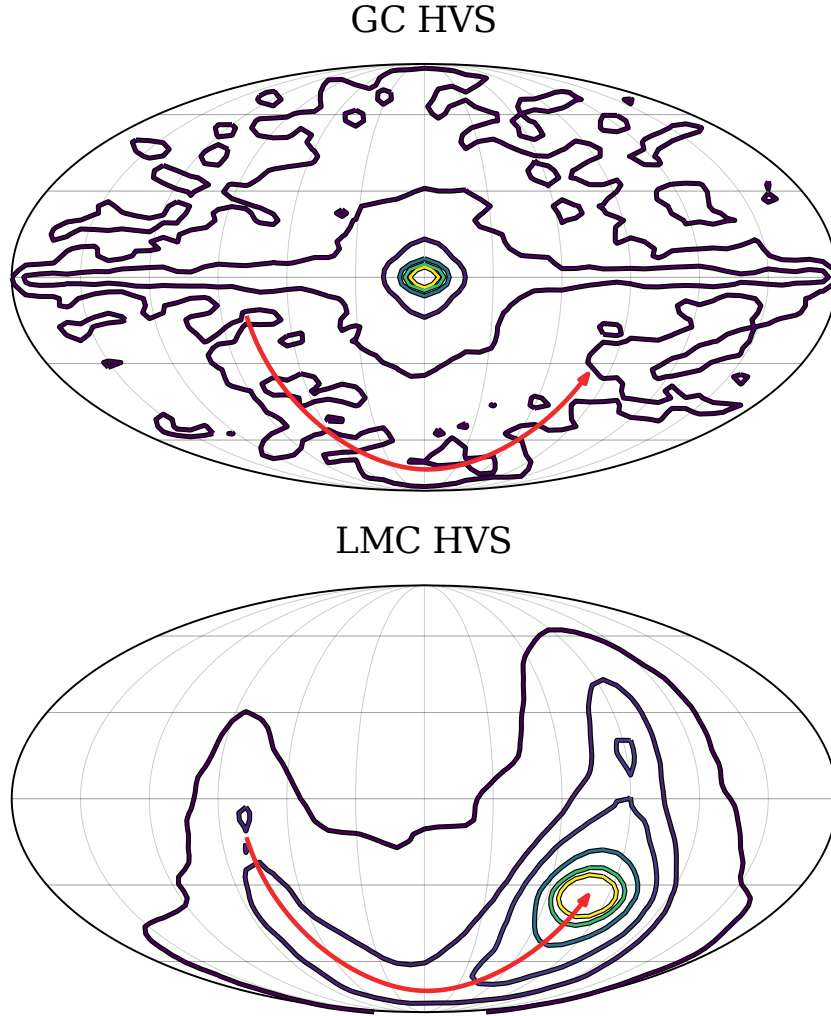


Figure 2. Density contours in Galactic coordinates using a Mollweide projection for HVSs ejected via the Hills mechanism from the Galactic Centre (left) and LMC centre (right). Contours are spaced logarithmically. The red curve shows the LMC trajectory on the sky over the last Gyr.

		N	mass (M_{\odot})	mag.	v_{GC} (km s $^{-1}$)	r_{GC} (kpc)	t_{age} (Myr)	$N_{unbound}$	$N_{v>500}$
<i>Gaia</i>	GC HVS	50^{+7}_{-8}	$2.6^{+1.1}_{-0.4}$	$17.8^{+2.0}_{-2.4}$	470^{+560}_{-340}	29^{+45}_{-22}	310^{+330}_{-210}	25 ± 6	24 ± 5
	LMC HVS	125^{+11}_{-12}	$2.4^{+0.7}_{-0.3}$	$19.5^{+0.8}_{-1.1}$	350^{+210}_{-90}	54^{+12}_{-15}	370^{+260}_{-200}	40^{+7}_{-8}	27 ± 6
LSST	GC HVS	42^{+6}_{-7}	$2.4^{+0.6}_{-0.3}$	$20.5^{+2.5}_{-3.1}$	630^{+530}_{-470}	64^{+180}_{-56}	420^{+300}_{-240}	30^{+5}_{-6}	27 ± 5
	LMC HVS	140^{+10}_{-11}	$2.3^{+0.6}_{-0.2}$	$20.2^{+1.7}_{-1.3}$	300^{+150}_{-80}	75^{+73}_{-29}	420^{+250}_{-220}	64^{+8}_{-7}	41 ± 7

Table 1. Properties of our *Gaia* and LSST samples of GC and LMC HVSs. The table summarizes their predicted number (N), median stellar masses, apparent magnitudes, Galactocentric velocities/distances, stellar ages, the number $N_{unbound}$ of HVSs gravitationally unbound to the Galaxy, and the number $N_{v>500}$ of stars with Galactocentric total velocities in excess of 500 km s $^{-1}$. Population counts assume an HVS ejection rate of 10^{-4} yr $^{-1}$ from both the GC and LMC. Quoted uncertainties span the 16th to 84th percentile and are calculated over 50 iterations. *Gaia* and LSST magnitudes are given in the *Gaia* G and LSST r bands, respectively.

4.1 Selecting *Gaia*- and LSST-detectable stars

In the left panel of Fig. 4 we show with solid lines the apparent magnitude distributions of $m > 0.5 M_{\odot}$ HVSs in the *Gaia* G band (solid lines). For its fourth and nominally final data release (DR4), *Gaia* aims to acquire five-parameter (5D) astrometric solutions as well as photometry for ~ 2 billion sources to a depth of $G \lesssim 20.7$ (see [Gaia Collaboration](#)

[et al. 2016a](#)). We select *Gaia* DR4-visible HVSs as simply all those brighter than this limit. We discuss the *Gaia* selection function in more detail in Sec. 6.3. As seen in Fig. 4, the vast majority of HVSs are fainter than $G = 20.7$. An HVS with the median stellar mass among our sample ($m \simeq 0.69 M_{\odot}$) must be closer than ~ 5 kpc to satisfy this limit. Since more massive ejected stars are much more likely to be detected (see below for more on this point), we show as well with dash-dotted

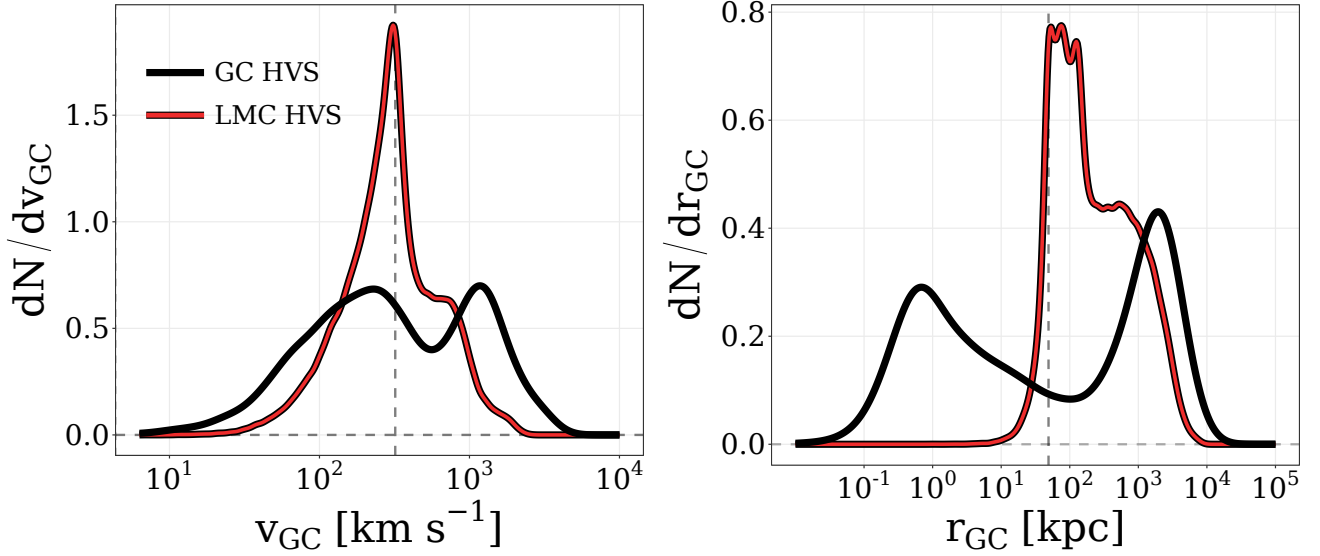


Figure 3. Distributions of Galactocentric velocities (left) and distances (right) for $m > 0.5 M_{\odot}$ HVSs ejected from the GC (black) and LMC (red) propagated through the MW+LMC potential. Vertical dashed lines show the Galactocentric velocity (320 km s^{-1}) and distance (49 kpc) of the LMC today.

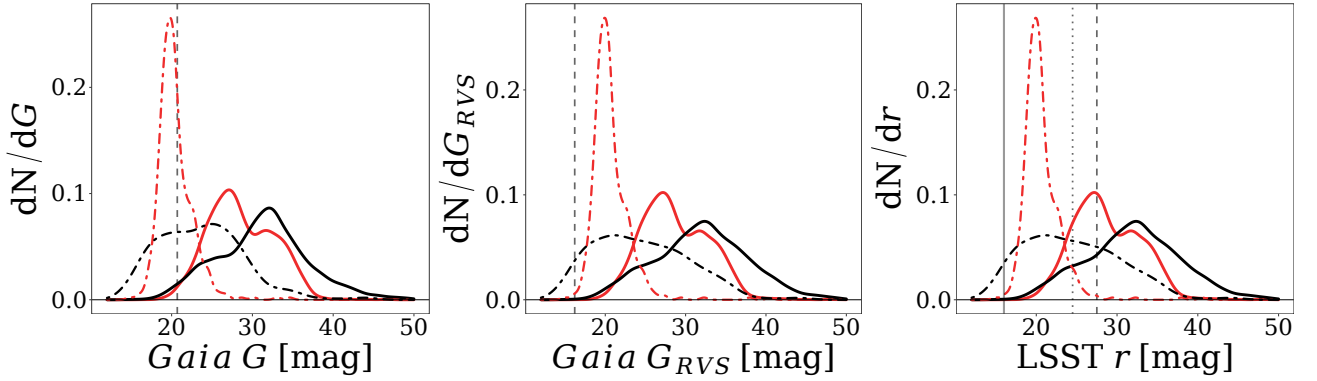


Figure 4. Apparent magnitude distributions for HVSs in the *Gaia* G (left), *Gaia* G_{RVS} (center) and LSST r (right) bands. Red and black curves show LMC HVS and GC HVS populations, respectively. Solid and dash-dotted curves show distributions for $m > 0.5 M_{\odot}$ and $m > 2 M_{\odot}$ HVSs, respectively. Dashed vertical lines in the left and center panels correspond to $G = 20.7$ and $G_{RVS} = 16.2$; the magnitude limits for the *Gaia* final data release five-parameter astrometric catalogue and the radial velocity catalogue, respectively. Solid, dotted and dashed vertical lines in the right panel correspond to $r = 16$, $r = 24.5$ and $r = 27.5$; the estimated LSST saturation limit, single-visit magnitude limit and ten-year coadded magnitude limit, respectively.

curves the distributions for GC and LMC HVSs more massive than $2 M_{\odot}$, which constitute $\sim 0.75\%$ of the total population. The apparent magnitude of a $2 M_{\odot}$ HVS at the position and distance of the LMC coincides roughly with the *Gaia* DR4 magnitude limit. Two thirds of $m > 2 M_{\odot}$ LMC HVSs and one third of $m > 2 M_{\odot}$ GC HVSs are brighter than this limit.

Gaia's on-board Radial Velocity Spectrometer (RVS) will provide radial velocity measurements for sources brighter than magnitude 16.2 in the *Gaia* G_{RVS} band (Katz et al. 2019). We show the apparent magnitude distributions of $m > 0.5 M_{\odot}$ and $m > 2 M_{\odot}$ HVSs in the center panel of Fig. 4. While ~ 5 per cent of $m > 2 M_{\odot}$ GC HVSs will be brighter than $G_{RVS} = 16.2$, this cut will exclude virtually all LMC HVSs. Additionally, as of Early Data Release 3, *Gaia* radial velocities are only validated for sources with effective temperatures [$3550 \text{ K} < T_{\text{eff}} < 6900 \text{ K}$], which corresponds

to a mass range of roughly [$0.5 M_{\odot} \lesssim m \lesssim 2 M_{\odot}$] given our assumptions. While the final *Gaia* data release will include radial velocities for hotter and cooler stars (Katz et al. 2019), the expected precision worsens at the hot end⁸. Given the inability of the *Gaia* DR4 6D survey to detect LMC HVSs, we will not discuss it further in this paper. GC HVSs which will appear in *Gaia* DR4 6D and the constraints they can offer on the properties of the GC stellar population will be the topic of an upcoming work.

LSST's primary 'wide-deep-fast' survey strategy will observe roughly 18,000 square degrees spanning $-65^{\circ} < \delta < +5^{\circ}$ to a single-visit depth of $r < 24.5$ and an estimated

⁸ see performance predictions here: <https://www.cosmos.esa.int/web/gaia/science-performance>

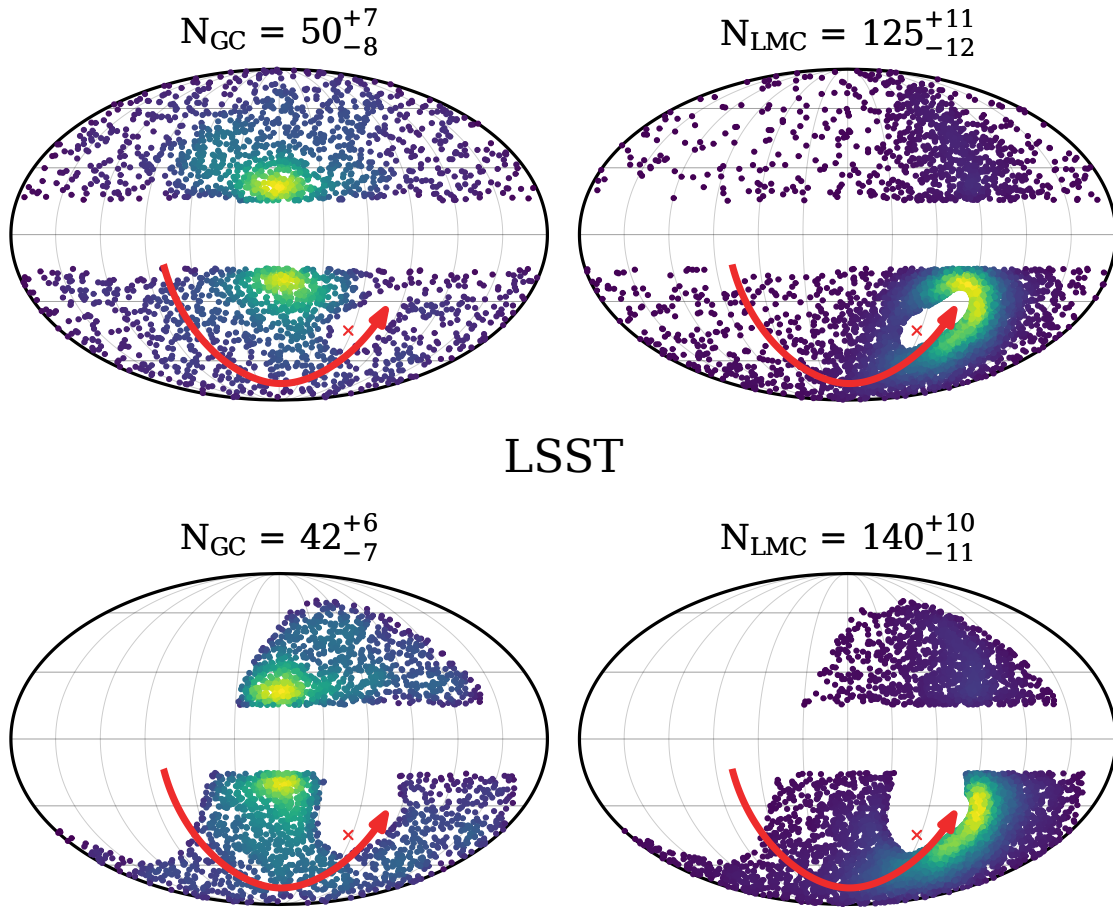
Gaia DR4 5D

Figure 5. Sky distributions of the GC HVS and LMC HVS populations in a Mollweide projection in Galactic coordinates. *Gaia* HVSs shown in upper panels, LSST HVSs in the bottom panels. See Sec. 4.1 for more information on the sample selection criteria. Annotations show the number of detectable GC and LMC HVSs in each sample assuming an HVS ejection rate of 10^{-4} yr^{-1} . Shown distributions are stacked over 50 iterations of the simulations. Points are linearly coloured by number density. The red curve shows the trajectory of the LMC on the sky over the last Gyr. The current position of the SMC is marked by a red ‘x’ for reference.

coadded depth of $r < 27.5$ after ten years of operation (see LSST Science Collaboration et al. 2017; Ivezić et al. 2019). We select LSST-detectable mock HVSSs as those brighter than the single-visit depth in this sky volume. We remove stars brighter than LSST’s saturation limit at $r = 16$ (Ivezić et al. 2019). The apparent magnitude distributions of HVSSs in the LSST r band are shown in the right panel of Fig. 4. 95 per cent of $m > 2 M_{\odot}$ LMC HVSSs and half of $m > 2 M_{\odot}$ GC HVSSs will satisfy $16 < r < 24.5$. These proportions rise to 98 per cent and 66 per cent respectively when considering $16 < r < 27.5$.

We caution that an HVS satisfying a particular survey’s selection criteria does not mean it will be easily *identifiable* as a genuine HVS. Many stars will be ejected at low velocities and remain confined to the crowded GC or inner LMC environments (Figs. 1, 2). Low-mass stars ejected to the Galactic stellar halo may be difficult to distinguish as they will likely have total velocities and spectral types typical of ordinary halo stars. In addition to the *Gaia* and LSST magnitude cuts described above, we additionally apply the following ones:

- Following the philosophy of the MMT Hypervelocity Star Survey (Brown et al. 2006, 2007, 2009a, 2012), we select only early-type stars at significant Galactic latitudes, $|b| > 15^{\circ}$ (see also Raddi et al. 2021). Given the lack of ongoing star formation in the stellar halo, early-type stars at faint magnitudes should not be seen at high latitudes and significant distances unless they were ejected there from their place of birth. We define early-type stars as $m \geq 2 M_{\odot}$ stars, corresponding roughly with stars of spectral type A1V or earlier (e.g. Pecaut & Mamajek 2013).

- To avoid confusion with ordinary bound stars in the inner LMC or Small Magellanic Cloud (SMC), we select only stars $> 10^{\circ}$ from the LMC centre, $> 10^{\circ}$ from the SMC centre and $> 10^{\circ}$ from any point on the line connecting the LMC centre and SMC centre on the sky. At the distance of the LMC this corresponds to a projected separation of ~ 9 kpc.

For brevity, in the remainder of this work we refer to our HVS samples that satisfy the above cuts as simply *Gaia* HVSs and LSST HVSs for stars within the *Gaia* DR4 5D and LSST magnitude limits respectively.

4.2 Properties of *Gaia* HVS samples

In Fig. 5, we show the sky distributions and expected numbers of our *Gaia* HVS samples (upper panels). We predict 50^{+7}_{-8} GC HVSs to be present in this catalogue along with 125^{+11}_{-12} LMC HVSs. We note that these estimates assume an HVS ejection rate from both the GC and LMC centre of 10^{-4} yr^{-1} – they should be scaled linearly to correspond to different ejection rate assumptions, should stricter constraints on these rates become known. While the LMC is at a larger heliocentric distance than the GC and ejects stars at a lower average velocity than the GC (see Fig. 1), its lower central escape velocity allows for its ejected stars to escape the inner LMC easily and reach observationally accessible regions of the sky. Therefore it is possible that LMC HVSs will greatly outnumber GC HVSs in *Gaia* DR4. The leading arm feature discussed in Sec. 3 is still visible, however, the most striking feature is the tight clump of LMC HVSs slightly leading the LMC orbit. We comment further on this feature later.

We summarize the main properties of *Gaia* HVSs in Table 1 and in Fig. 6 we show their distributions of in stellar mass, *Gaia* *G*-band apparent magnitude, Galactocentric distance and velocity, and stellar age. The main differences between LMC and GC HVSs are their apparent magnitudes and Galactocentric distance and velocity distributions. GC HVSs outnumber LMC HVSs by a factor of 2.2 when considering only HVSs brighter than $G = 18$. While LMC HVSs are more concentrated around the Galactocentric distance and total orbital velocity of the LMC, GC HVSs have broader distributions, peaking at lower values but showing significant tails towards large distances and velocities. Roughly half (24 ± 5) of the GC HVSs have total velocities in excess of 500 km s^{-1} , while for LMC HVSs this percentage decreases to $\sim 20\%$ (27^{+5}_{-5} stars).

4.2.1 *Gaia* astrometric errors

We use *PyGaia* to characterize the estimated *Gaia* end-of-mission astrometric errors of these populations. The median relative parallax error for *Gaia* GC HVSs is 370 per cent. Of the 50^{+7}_{-8} GC HVSs predicted to appear in *Gaia*, only 5 ± 1 will have a relative parallax error below 20 per cent; the relative error above which estimating distances becomes non-trivial (Bailer-Jones 2015). LMC HVSs manage even worse, with a median relative parallax error of 1820 per cent. We do not predict a single LMC HVS to be present among our *Gaia* HVSs with a relative parallax error below 20 per cent.

By contrast, the proper motion measurements provided by *Gaia* will be more reliable. The median relative uncertainty on the proper motion magnitude for GC HVSs is 6.4 per cent. 23^{+4}_{-3} GC HVSs will appear in *Gaia* with proper motion uncertainties below 5 per cent, alike in number to the 18^{+2}_{-2} LMC HVSs with similar uncertainties.

4.3 Properties of LSST HVS samples

The spatial distribution of our LSST HVS populations are shown in Fig. 5, lower panels. We predict 42^{+6}_{-7} GC HVSs, significantly outnumbered by the 140^{+10}_{-11} LMC HVSs. While LSST faint-end magnitude limit will be deeper than *Gaia*, its HVS-hunting abilities are hamstrung by the fact that nearly

the entirely equatorial north is inaccessible to it. If we consider LSST’s ten-year estimated coadded depth of $r < 27.5$ rather than its single-visit depth of $r < 24.5$, we predict 142^{+10}_{-12} LMC HVSs and 47^{+7}_{-8} GC HVSs. Most $m > 2 M_{\odot}$ GC HVSs and nearly all $m > 2 M_{\odot}$ LMC HVSs already satisfy $r < 24.5$ (see Fig. 4), so the fainter limit does not translate to significantly more detectable HVSs. LSST’s fainter limit does not imply superior astrometric errors when compared to *Gaia*: *Gaia* proper motion and parallax errors will be superior to LSST for sources $r \lesssim 20$ and LSST smoothly extends *Gaia*’s error-versus-magnitude curve for $r > 20$ (Ivezić et al. 2012).

Table 1 and Fig. 7 summarize the properties of our LSST HVS samples. We see similar trends as in Fig. 6. Owing to its fainter magnitude limit, LSST GC HVSs in particular will be found at farther Galactocentric distances and faster total velocities than those found in *Gaia*. LMC HVSs remain concentrated at Galactocentric total velocities similar to the LMC’s orbital velocity and distances slightly farther than the LMC. For LSST, $\sim 60\%$ (30%) of GC (LMC) HVSs have total velocities faster than 500 km s^{-1} , higher proportions than was the case for *Gaia*.

We point out that a significant fraction of detectable HVSs will be gravitationally unbound to the MW. The blue curve in the v_{GC} vs. r_{GC} panel of Figs. 6 and 7 (fourth row, third column) shows the escape velocity from our default MW+LMC potential along the line connecting the GC and the present-day LMC centre. Roughly half (25 ± 6) of *Gaia* GC HVSs and \sim one third (40^{+7}_{-8}) LMC HVSs will be unbound to the Galaxy. These proportions rise to 70 per cent (30^{+5}_{-6}) and 46 per cent (64^{+8}_{-7}) respectively for our LSST HVS sample (see Table 1).

4.4 The LMC HVS leading overdensity

Fig. 5 shows that many of the LMC HVSs visible by *Gaia* and LSST are found in a feature slightly leading the LMC orbit. We focus further on this overdensity by selecting only the HVSs between 10° and 25° from the LMC centre and $>10^{\circ}$ from the SMC centre. This 25° limit corresponds to a projected distance of 22 kpc from the LMC centre and is more or less the ballistic travel distance of a $2 M_{\odot}$ HVS with the median ejection velocity from the LMC and median flight time in our fiducial model (102 km s^{-1} and 162 Myr respectively). Note that the LSST wide-deep-fast survey strategy will not cover this entire region as it extends slightly south of the $\delta = -65^{\circ}$ survey edge. While stars in this bow overdensity would be sufficiently well-separated from the LMC to not be confused with inner LMC stars, they may overlap on the sky with structures seen in the LMC outskirts (see e.g. *Gaia* Collaboration et al. 2020). In particular it may overlap the stream-like feature due north of the LMC reported by Mackey et al. (2016), though this feature is comprised predominantly of old stars.

We show in Fig. 8 the sky distribution and number of stars located in this feature. We show as well the distribution in an orthographic projection centred on the LMC (see also *Gaia* Collaboration et al. 2018, 2020). Of the 125^{+11}_{-12} *Gaia* LMC HVSs, 58^{+6}_{-7} are located in this bow overdensity feature and a similar number is expected with LSST (48 ± 6). Contamination from GC HVSs in this region is modest, up to just a few assuming an ejection rate of 10^{-4} yr^{-1} . Targeting can-

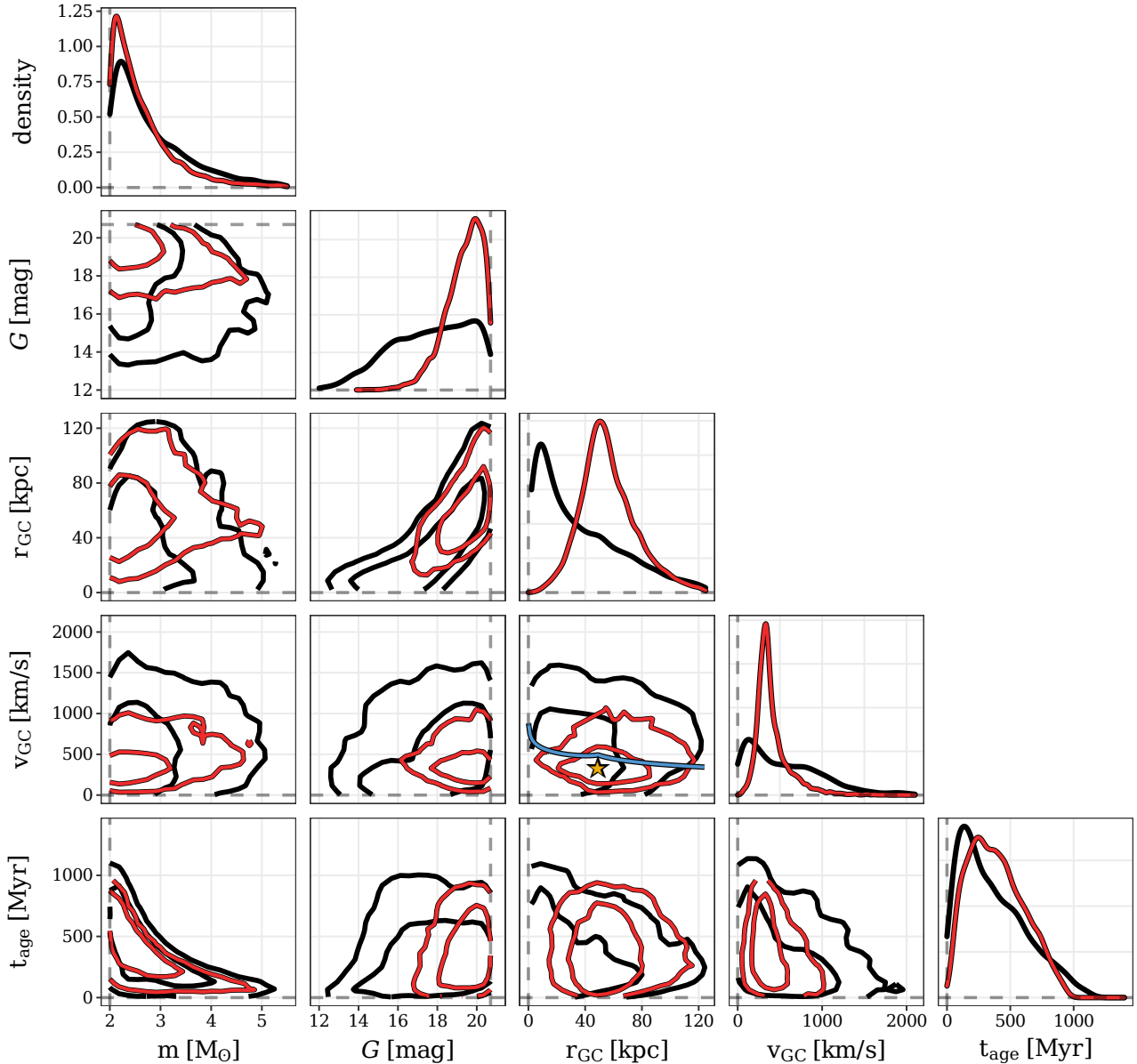


Figure 6. *Gaia* HVS samples’ distributions of and between stellar mass m , *Gaia* G -band magnitude, Galactocentric distance r_{GC} , Galactocentric total velocity v_{GC} and stellar age t_{age} . LMC HVS distributions are shown in red and GC HVSs in black. Contours show 68th and 95th percentiles of the distributions. The blue curve in the v_{GC} vs. r_{GC} plot (fourth row, third column) shows the escape velocity to infinity from the MW+LMC potential today along the vector connecting the GC and the LMC centre. The velocity and distance of the LMC is denoted by the gold star.

didates in this feature in either survey for follow-up observations would therefore maximize one’s chances of finding genuine LMC HVSSs, while minimizing contamination from interloping GC HVSSs.

5 IMPACT OF MW+LMC POTENTIAL ASSUMPTIONS

The maps and number estimates shown in Fig. 5 and Table 1 are for the default ejection model and MW+LMC potential summarized in Sec. 2.3. In this subsection we run additional simulations to explore the sensitivity of these predictions to

changes in our assumptions concerning the LMC MBH mass and our MW+LMC potential.

We explore additional LMC MBH masses of $M_{MBH,LMC} = [10^{3.6}, 10^4, 10^6, 10^{7.1}] M_{\odot}$. This lower limit is based on the ejection velocity of HVS3 (Erkal et al. 2019a) and the upper limit based on Boyce et al. (2017), who use line-of-sight velocity maps from MUSE observations to constrain the LMC MBH mass. An increase in $M_{MBH,LMC}$ affects the trajectories of LMC HVSSs and leads to a larger high-velocity tail in ejection velocities (see Eq. 1). The median ejection velocity from a $M_{MBH,LMC} = 10^{7.1} M_{\odot}$ MBH increases to 440 km s^{-1} compared to the median ejection velocity of 200 km s^{-1} from our default $M_{MBH,LMC} = 10^5 M_{\odot}$ MBH.

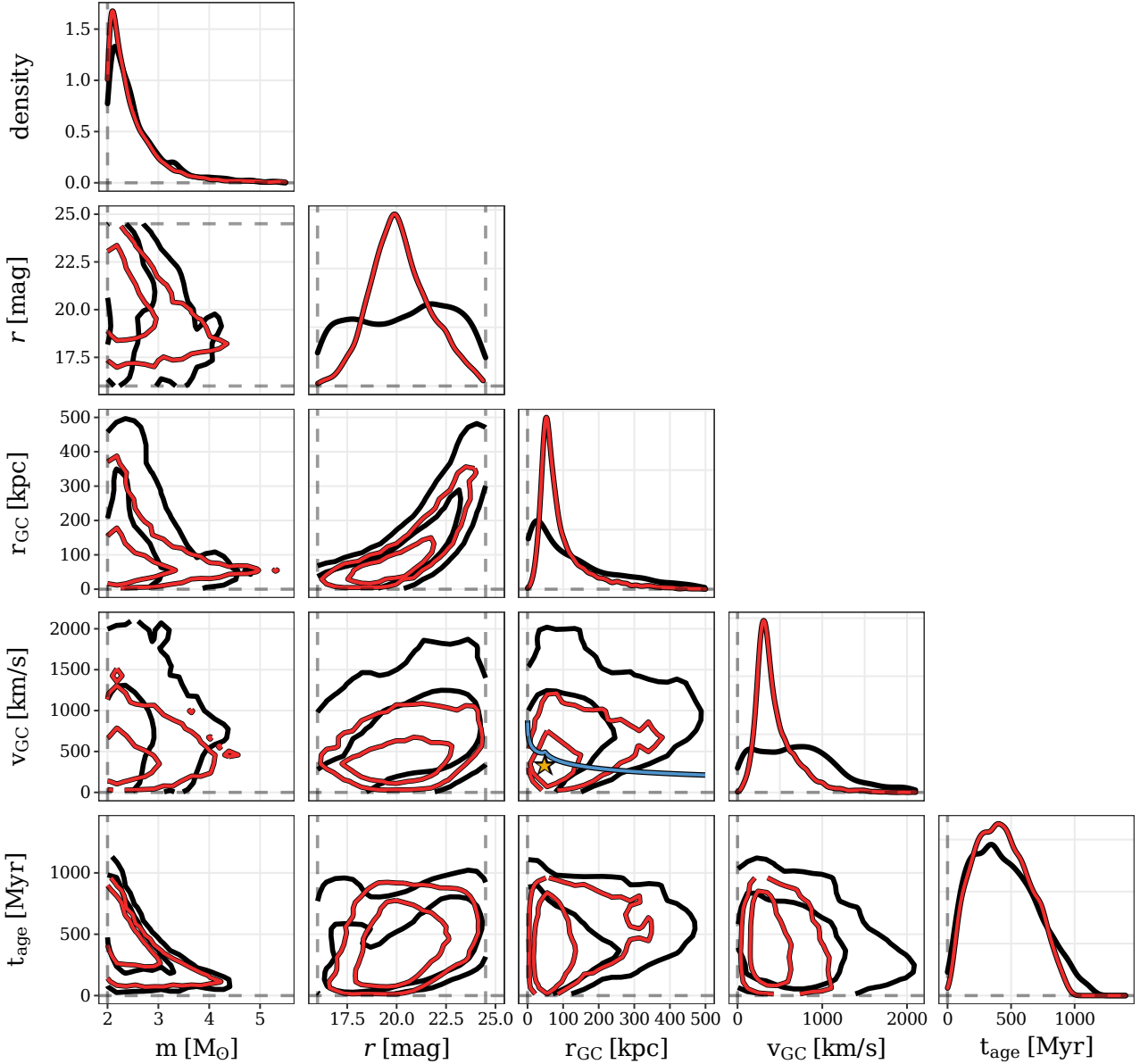


Figure 7. Same as Fig. 6 but for the LSST samples. Apparent magnitudes are shown in the LSST r band.

When considering different LMC masses, we explore $M_{\text{LMC}} = [2, 5, 10, 20, 25] \times 10^{10} M_{\odot}$ similar to Belokurov et al. (2019). The lower limit is based on the enclosed mass constraints within 8.7 kpc inferred by van der Marel & Kallivayalil (2014) via rotation measurements. The upper limit is based on the LMC mass determined by Peñarrubia et al. (2016) based on the impact of the LMC on the MW-M31 timing argument. We set a different LMC scale radius for each scale mass, requiring that the circular velocity at 8.7 kpc from the LMC centre is 91.7 km s^{-1} (van der Marel & Kallivayalil 2014).

While the Galactic disc and bulge potentials remain fixed in all models, we consider changes in the Galactic dark matter halo. We explore spherical NFW halos ($c_{\text{halo}}=1$) with r_s fixed and $M_s=[0.5, 2, 3, 4] \times 0.76 \times 10^{12} M_{\odot}$, as well as

oblate/prolate spheroids with M_s and r_s fixed at their fiducial values but $c_{\text{halo}}=[0.6, 0.8, 1.2, 1.4]$.

In Fig. 9 we show how the numbers of *Gaia* and LSST HVSs depend on the the above parameters. Both the predicted number of GC HVSs (N_{GC}) and LMC HVSs (N_{LMC}) are fairly agnostic towards M_{halo} . The number of LSST HVSs ejected from both the GC and LMC declines slightly with increasing M_{halo} . A heavier halo implies a larger escape velocity from the inner Milky Way and therefore a reduced number of GC HVSs reaching observationally accessible locations on the sky. However, a larger deceleration from the GC to the Galactic halo reduces the typical heliocentric distance of GC HVSs at time of observation, increasing the number of brighter sources within the *Gaia* or LSST horizons. As M_{halo} increases, the LMC has spent a larger fraction of its recent past close to the MW, so stars with larger flight times become

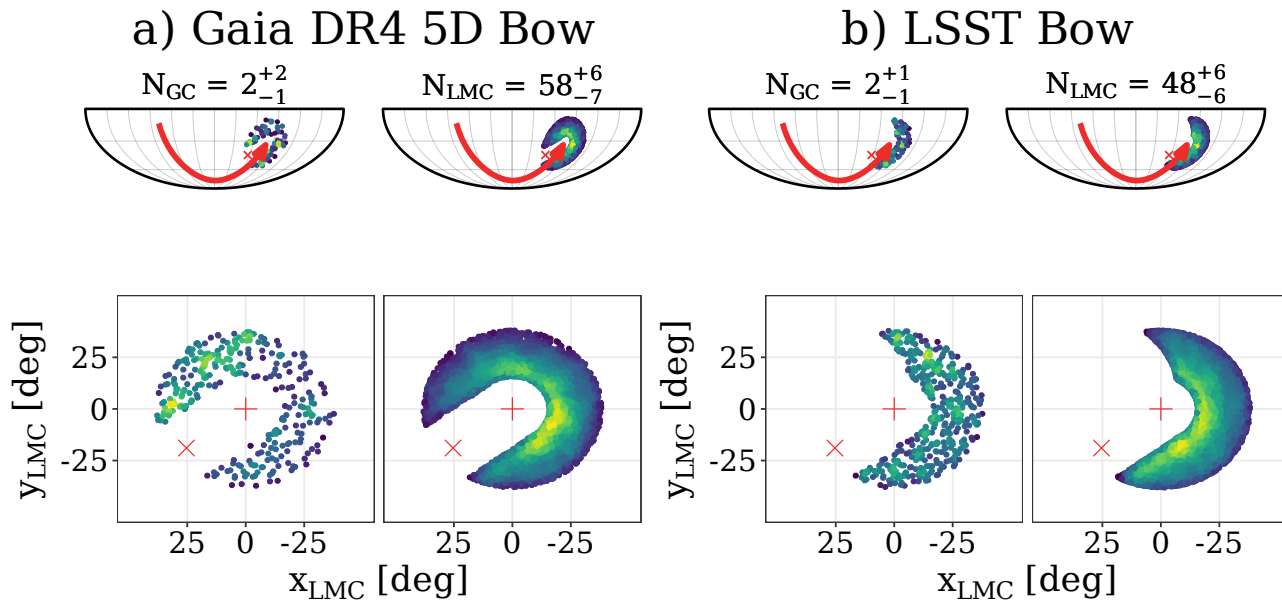


Figure 8. *Top row:* Same as Fig. 5 but showing only GC HVSs and LMC HVSs in the bow overdensity leading the LMC orbit, i.e. $>10^\circ$ from both the LMC and SMC but $<25^\circ$ from the LMC. Distributions are shown for stars which would appear in a) *Gaia* and b) LSST samples. Annotations show the number of GC and LMC HVSs present in this feature assuming an LMC HVS ejection rate of 10^{-4} yr^{-1} . *Bottom row:* Same as top row but in an orthographic projection centred on the LMC centre in equatorial coordinates. Red cross and ‘x’ symbols denote the positions of the LMC and SMC in this projection, respectively.

bright enough to be detected. Additionally, as with N_{GC} , a larger enclosed mass implies fewer LMC HVSs on outbound orbits reach Galactocentric distances beyond the *Gaia* horizon.

We see in Fig. 9 that increasing $M_{\text{BH,LMC}}$ increases the number of LSST LMC HVSs. The number of *Gaia* LMC HVSs increases mildly with $M_{\text{BH,LMC}}$, peaking near $M_{\text{BH,LMC}} \simeq 10^5 M_\odot$ before turning over. Recall from Eq. 1 that the Hills mechanism ejection velocity scales as $\propto M_{\text{BH}}^{1/6}$ – an order of magnitude increase in M_{BH} scales v_{ej} by a factor of ~ 1.5 . A more massive LMC MBH is more effective at ejecting stars which leave the inner LMC, but simultaneously ejects more stars which reach heliocentric distances beyond the *Gaia*/LSST horizons before being observed.

We see in Fig. 9 that N_{GC} and N_{LMC} are quite flat with M_{LMC} . In the M_{LMC} range we probe, the LMC remains far sub-dominant to the MW in its contribution to the MW+LMC potential. A modest increase in M_{LMC} does not appreciably affect the fraction of LMC HVSs which escape the inner LMC. While the LMC mass impacts the perturbation of GC HVSs by the LMC (see Kenyon et al. 2018), its impact on the absolute number of observable GC HVSs is negligible. We note that even when the LMC scale radius is kept fixed, N_{GC} and N_{LMC} do not vary with increasing M_{LMC} .

Finally, we show in Fig. 9 the impact of the flattening of the Galactic dark matter halo. $c_{\text{halo}} < 1$ and $c_{\text{halo}} > 1$ correspond to an oblate and a prolate halo, respectively. While N_{LMC} is quite flat with c_{halo} , N_{GC} overall increases mildly with increasing c_{halo} for both *Gaia* and LSST HVS populations. While different halo flattenings affect the trajectories of individual stars and the orbital history of the LMC,

its impact on the number of detectable HVSs is quite small. The deflection caused by an oblate halo may bring more GC HVSs towards the Galactic midplane and thus not satisfy our $|b| > 15^\circ$ cut. This is the most likely explanation for the slight increase of N_{GC} with c_{halo} .

In summary, while the model parameters explored above impact the trajectories and detectability of individual stars, the absolute numbers of GC HVSs and LMC HVSs observable by *Gaia* and LSST are relatively robust against variation of these parameters. Marginalizing over these explored parameters in the ranges explored assuming flat priors for M_{halo} , c_{halo} , M_{LMC} and a log-flat prior for $M_{\text{BH,LMC}}$, we obtain N_{GC} and N_{LMC} predictions quite close to the estimates of our fiducial model.

6 DISCUSSION

In this section we comment on a number of considerations related to our predictions and on caveats which may impact the expected number and characteristics of GC and LMC HVSs.

6.1 Comparison with known HVS candidates

HVS3 was discovered by Edelmann et al. (2005) while performing a spectroscopic follow-up of faint B-type star candidates from the Hamburg/ESO survey. This is the only HVS candidate currently associated with an origin in the LMC centre (Erkal et al. 2019a). It appears in *Gaia* DR2 with an apparent magnitude of $G = 16.4$, but would not have been kinematically identified as a promising HVS candidate from

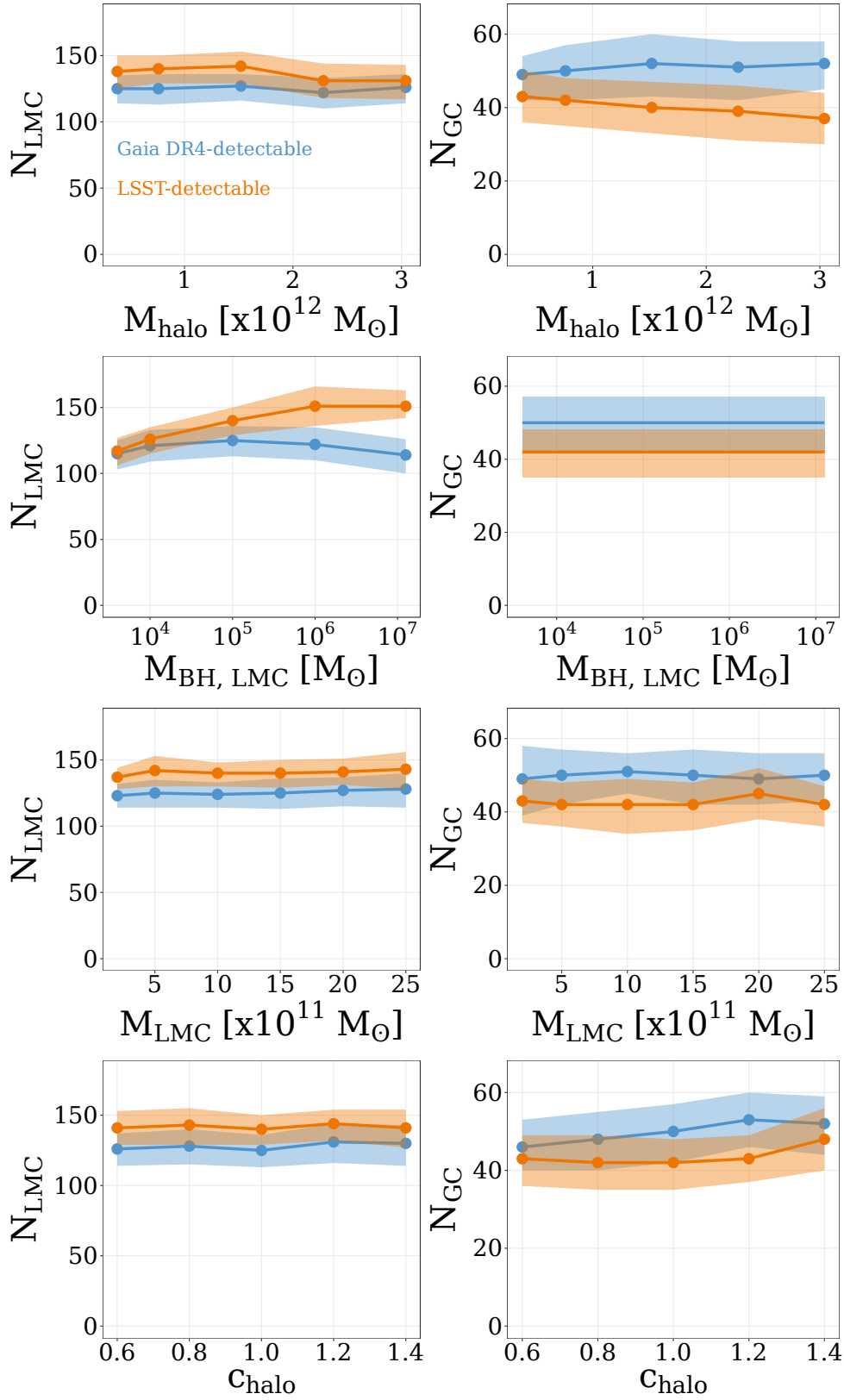


Figure 9. The dependence of the numbers N_{LMC} and N_{GC} of *Gaia*-detectable and LSST-detectable GC HVSs and LMC HVSs on model assumptions. N_{LMC} (left column) and N_{GC} (right column) are shown against the scale mass of the MW dark matter halo (top row), the mass of the LMC central MBH (second row), the LMC scale mass (third row), MW dark matter halo flattening (fourth row). Shaded region show 1σ confidence intervals.

Gaia data alone, as it lacks a reliable parallax measurement and does not appear in the *Gaia* subsample with published radial velocities.

HVS3 is a $8 \pm 1 M_{\odot}$ star located at $\alpha = 69.6^{\circ}$, $\delta = -54.6^{\circ}$ (Przybilla et al. 2008). This place is coincident with the bow overdensity feature leading the LMC orbit shown in Fig. 8. While its distance and total velocity are typical of other $m > 5 M_{\odot}$ stars located in this feature, according to our results it is quite a rare and exceptional object. At an assumed LMC HVS ejection rate of 10^{-4} yr^{-1} , we predict that *Gaia* DR4 will contain $1.5^{+1.4}_{-0.9}$ LMC HVSs with masses greater than $5 M_{\odot}$ in this bow feature, and we find a 6 per cent chance for it to contain a $m \geq 8 M_{\odot}$ star. While not incompatible with our predictions, the presence of HVS3 in *Gaia* could hint that our LMC HVS ejection rate assumption of 10^{-4} yr^{-1} errs to the conservative side. If the true LMC HVS ejection rate is a factor of \sim a few larger than assumed here, the existence of an HVS3-like object becomes much less unlikely. Alternatively, the initial mass function in the LMC centre may be more top-heavy than assumed in this work. For instance, the probability of *Gaia* DR4 containing an HVS3-like object in the leading overdensity doubles to ~ 12 per cent if the stellar IMF in the innermost pc of the LMC has a power-law slope of -1.7 similar to the IMF in the innermost 0.5 pc of the Milky Way found by Lu et al. (2013).

Equally exceptional as HVS3 is the confirmed GC HVS S5-HVS1 (Koposov et al. 2020). While first identified in the S⁵ survey (Li et al. 2019), S5-HVS1 appears in *Gaia* DR2 with an apparent magnitude of $G = 16.0$ and without a reliable parallax measurement or radial velocity measurement. At $\alpha = 343.7^{\circ}$, $\delta = -51.2^{\circ}$, it is located just south of the GC HVS overdensity in the Galactic south seen in Fig. 5. S5-HVS1 has a breakneck estimated ejection velocity ($v_{\text{ej}} \simeq 1800 \text{ km s}^{-1}$) and relatively short flight time ($t_{\text{flight}} \simeq 4.8 \text{ Myr}$). We do not predict future *Gaia* data releases to contain a sizeable population of S5-HVS1-like objects – we expect *Gaia* DR4 to contain only $1.6^{+1.4}_{-0.9}$ GC HVSs with $v_{\text{ej}} > 1500 \text{ km s}^{-1}$ and $t_{\text{flight}} < 20 \text{ Myr}$.

We finally consider the HVS candidates in the MMT HVS Survey (Brown et al. 2012), gathered from a targeted search of early-type stars in the Galactic halo. In particular, we consider the 12 HVS candidates whose distribution of possible Galactic plane-crossing locations include the GC at the 1σ level (c.f. Kreuzer et al. 2020, fig. 8). Like HVS3 and S5-HVS1, these objects all appear in *Gaia* DR2 without radial velocities. They are quite distant ($50 \text{ kpc} \lesssim d \lesssim 160 \text{ kpc}$) – with such long flight times and large relative astrometric uncertainties, the range of possible plane-crossing locations becomes naturally quite extended, often many times larger than the size of the Galactic disc. Because our expected GC HVS sample peaks at distances much smaller than 50 kpc (see Table 1 and Fig. 6), these 12 known candidates would constitute a substantial fraction of the 15^{+4}_{-3} GC HVSs we predict to appear in *Gaia* DR4 at heliocentric distances in excess of 50 kpc.

6.2 HVS ejection rates from the GC and LMC centre

HVS ejection rates are derived and constrained from different angles: theoretical estimates (e.g. Hills 1988; Yu & Tremaine 2003), detailed simulations (Zhang et al. 2013), comparisons to known HVS candidates (e.g. Bromley et al. 2012; Brown

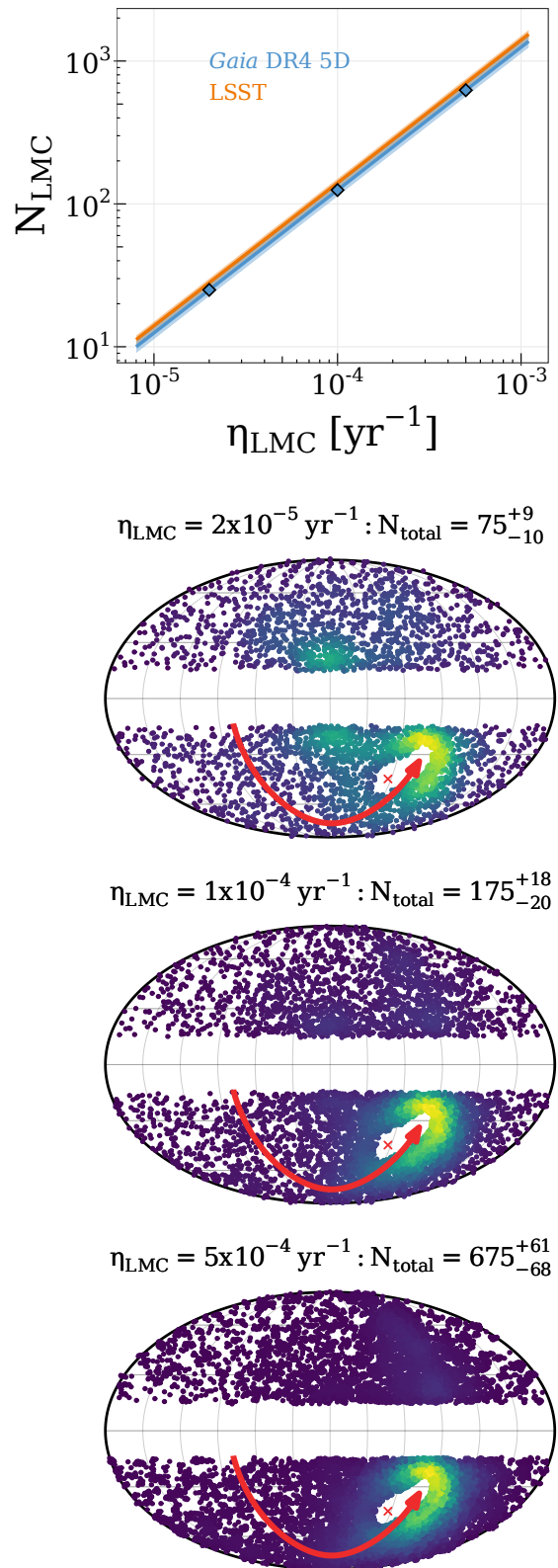


Figure 10. *Top:* Dependence of N_{LMC} on the LMC HVS ejection rate η_{LMC} for HVSs detectable by both *Gaia* and LSST. *Sec-ond, third and fourth from top:* Similar to Fig. 5 but for the combined GC+LMC HVS population detectable in *Gaia* DR4. Different η_{LMC} values are assumed in each panel corresponding to the plotted points in the top panel, while the GC HVS ejection rate is fixed at 10^{-4} yr^{-1} .

et al. 2014; Marchetti et al. 2018), observations of the Galactic S star cluster (Bromley et al. 2012) and tidal disruption event rates in the local Universe (e.g. Wang & Merritt 2004; Gezari et al. 2009; Bromley et al. 2012; van Velzen & Farrar 2014). Overall, these methods indicate an HVS ejection rate in the range $\sim 10^{-5} - 10^{-3} \text{ yr}^{-1}$. For simplicity, in this work we adopt a constant HVS ejection rate of 10^{-4} yr^{-1} for both the Milky Way and the LMC, so that a sample comparison is more straightforward. However, it might not be a realistic description. For example, the HVS ejection rate may scale inversely with the mass of the central black hole as the tidal disruption event rate does (see Stone & Metzger 2016). In this case the HVS ejection rate in the LMC would be greater than in the GC, further increasing the predicted dominance of LMC HVSs over GC HVSs in *Gaia* and LSST catalogues.

We demonstrate the importance of the still-uncertain LMC HVS ejection rate η_{LMC} in Fig. 10. In the top panel we illustrate how N_{LMC} for both *Gaia* and LSST HVSs change linearly with η_{LMC} . By comparison with Fig. 9, it is clear that η_{LMC} impacts our predictions more strongly than any assumption regarding the LMC MBH mass or the MW+LMC potential. In the remaining panels of Fig. 10 we show the sky distribution of the combined *Gaia* GC and LMC HVS population for different η_{LMC} assumptions while the GC HVS ejection rate is fixed at 10^{-4} yr^{-1} . It is clear that a significant change in η_{LMC} greatly influences the size of the total HVS population and its distribution. If stricter constraints on the LMC HVS ejection rate become available, our predictions can be scaled accordingly. However, our characterizations of the spatial distributions of the individual LMC HVS and GC HVS populations and their kinematics and properties remain valid as they are independent of the assumed HVS ejection rate.

6.3 The *Gaia* and LSST selection functions

Throughout this work we have assumed that the *Gaia* DR4 catalogue with five-parameter astrometry will be 100 per cent complete for $G < 20.7$ and entirely incomplete for fainter magnitudes, and similarly for LSST in the range $16 < r < 24.5$ in its survey volume. Though the precise selection functions of these future surveys cannot be predicted exactly, one may worry that the above assumptions are overly simplistic. For instance, because the *Gaia* astrometric pipeline requires a source be detected a minimum number of times to be included in the catalogue (Lindegren et al. 2018, 2021), the *Gaia* completeness function depends on the spinning-and-precessing scanning law of the satellite (see Boubert et al. 2020a). *Gaia* completeness is also impacted in regions of high crowding (Boubert & Everall 2020), however, this is not worrisome in the context of our results since we omit the most crowded regions of the sky (i.e. the inner LMC and Galactic midplane) from our analysis.

We consider the validity of our *Gaia* DR4 selection function approximation by comparing it to a more robust approximation, leveraging the known properties of the *Gaia* EDR3 selection function. We assume the following:

- The $G \leq 21$ and $\text{VISIBILITY_PERIODS_USED} \geq 9$ requirements for a source to have a full five-parameter astrometric

solution⁹ in *Gaia* EDR3 (Lindegren et al. 2021) remain unchanged for the DR4 astrometric pipeline.

- The *Gaia* DR4 source catalogue is not substantially more complete than EDR3 for $G \leq 21$, i.e. DR4 will not contain many sources which do not already appear in EDR3 with at least a two-parameter astrometric solution.
- Given that DR4 will be based on observations spanning a time period double that of EDR3, nearly all $G \leq 21$ sources in EDR3 will satisfy $\text{VISIBILITY_PERIODS_USED} \geq 9$ in DR4 (c.f. fig. 3 Fabricius et al. 2021).

If the above assumptions hold, the selection function for the *Gaia* DR4 subsample with five-parameter astrometry can be well-approximated by the $G \leq 21$ selection function of the *Gaia* EDR3 source catalogue. If we apply the EDR3 selection function provided by the PYTHON package SELECTION-FUNCTIONS¹⁰ based on Boubert & Everall (2020) to our mock HVS populations, we end up with only 6% more GC HVSs and 10% more LMC HVSs in *Gaia* DR4. For the purposes of this work, our simple $G < 20.7$ cut can therefore be considered a reasonable and conservative approximation to the *Gaia* DR4 astrometric selection function, missing the small fraction of HVSs fainter than the nominal completeness limit.

6.4 The reflex motion of the Milky Way in response to the LMC

Throughout this work we have assumed a reference frame in which the MW is fixed and the LMC orbits around it. With a mass \sim one tenth the mass of the MW, the LMC not only deflects the orbits of GC HVSs (Kenyon et al. 2018) but additionally perturbs the MW and induces a reflex motion of the MW centre of mass. Gómez et al. (2015) show that as a result of the LMC, the MW centre of mass within 50 kpc has been displaced by as much as 30 kpc and 75 km s^{-1} over the last $\sim 0.3 - 0.5 \text{ Gyr}$. Among other impacts, this reflex motion will affect the long-term orbital history of the LMC, the tidal disruption of the Sagittarius dwarf galaxy (Gómez et al. 2015), and the apparent motions within the outer stellar halo (Garavito-Camargo et al. 2019; Petersen & Peñarrubia 2020; Erkal et al. 2020).

In the context of HVSs, Boubert et al. (2020b) study the influence of this reflex motion on GC HVS trajectories. They find this reflex motion deflects the apparent trajectories of HVSs on the same order as the deflection induced by the LMC's influence itself. Disentangling these two effects, however, requires proper motion measurements precise to $10 \mu\text{as yr}^{-1}$, which would be possible in the proposed *Gaia* successor mission *Gaia*NIR (Hobbs et al. 2016).

Due to this reflex motion, it may be more difficult to conclusively associate GC HVSs with a GC origin, as their past trajectories will reflect the fact that they were ejected from the past GC location rather than the location of the GC today. Despite this, since most GC and LMC HVSs have flight times within a few hundred Myr and Galactocentric distances within a \sim few tens of kpc, the number of GC-ejected and LMC-ejected *Gaia* HVSs or LSST HVSs will not be significantly impacted by this phenomenon.

⁹ A *Gaia* visibility period is a group of astrometric observations separated from other groups by a time period of at least four days.

¹⁰ <https://github.com/gaiaverse/selectionfunctions>

6.5 Contamination by LMC hyper-runaways

Interaction with an MBH is not the only mechanism by which stars can obtain significant peculiar velocities. Dynamical ejections from young, dense stellar clusters (see [Poveda et al. 1967](#); [Leonard & Duncan 1990](#); [Leonard 1991](#)) and binary disruptions following core-collapse supernovae (e.g. [Blaauw 1961](#); [Tauris & Takens 1998](#); [Renzo et al. 2019](#)) are often blamed for the known population of main sequence ‘runaway stars’ with ejection velocities $\geq 30\text{--}40\text{ km s}^{-1}$ ([Blaauw 1961](#)). Both mechanisms are known, however, to struggle to eject enough stars at $\geq 450\text{--}500\text{ km s}^{-1}$ to explain the known population of main sequence ‘hyper-runaway’ stars ejected from the Galactic disc ([Portegies Zwart 2000](#); [Perets & Šubr 2012](#); [Oh & Kroupa 2016](#); [Evans et al. 2020](#)).

With its lower escape speed and its significant orbital velocity, however, the LMC disc might be more effective at ejecting main sequence runaway stars which escape the inner LMC. [Boubert et al. \(2017\)](#) explore the prospect of LMC hyper-runaways ejected via binary supernovae using the binary evolution code `binary_c` ([Izzard et al. 2009](#)) and an N-body MW+LMC potential. Their results indicate that at least as many early-type LMC hyper-runaways as HVSs may escape from the inner parts of the LMC and be detectable by *Gaia*. It may be difficult, then, to distinguish LMC HVSs from hyper-runaway stars ejected from the LMC disc. A quantitative assessment of this is beyond the scope of this paper and is deferred to a future dedicated work.

7 SUMMARY AND CONCLUSION

In this work we perform a suite of simulations ejecting hyper-velocity stars from the centres of the MW and the LMC via dynamical interactions between their central massive black holes and nearby binary systems. By propagating these stars through the Galactic potential and obtaining mock observations, we predict and characterize the GC HVS and LMC HVS populations visible in the near future by the *Gaia* mission in its fourth and final data release (DR4) as well as by the LSST survey. We restrict our predictions to stars which would be conspicuous as promising HVS candidates, i.e. early-type ($m > 2M_{\odot}$) stars well-separated on the sky from the Magellanic Clouds and the Galactic midplane. Our findings are summarized as follows:

- While the HVS ejection rate from the LMC remains uncertain, we predict 125^{+11}_{-12} LMC HVSs will be included in *Gaia* DR4 with five-parameter astrometric solutions assuming an HVS ejection rate of 10^{-4} yr^{-1} . These will greatly outnumber the 50^{+7}_{-8} GC HVSs we expect to be present in *Gaia* DR4. One half of GC HVSs and 22 per cent of LMC HVSs will have total velocities in excess of 500 km s^{-1} (see [Table 1](#) and [Fig. 6](#)).

- We do not predict any LMC HVSs to be present in the *Gaia* DR4 radial velocity catalogue due to its shallower magnitude limit ($G_{\text{RVS}} < 16.2$) and the restrictions on stellar effective temperature in the *Gaia* spectroscopic pipeline.

- Within LSST’s wide-deep-fast survey volume there will be 42^{+6}_{-7} GC HVSs and 141^{+10}_{-11} LMC HVSs within its magnitude limits. Median Galactocentric total velocities for these objects will be $630^{+530}_{-470}\text{ km s}^{-1}$ and $300^{+150}_{-80}\text{ km s}^{-1}$, respectively. 64 per cent of GC HVSs and 29 per cent of LMC HVSs

will have total velocities faster than 500 km s^{-1} (see [Table 1](#) and [Fig. 7](#)).

- GC HVSs and LMC HVSs will differ starkly in their spatial distribution ([Figs. 2](#) and [5](#)), concentrated mainly towards the Galactic meridian and outer LMC regions, respectively. LMC HVSs in particular will be preferentially found in a feature $< 25^{\circ}$ from the LMC leading its orbit ([Fig. 8](#)). \sim one half of *Gaia*-detectable LMC HVSs and one third of LSST-detectable LMC HVSs will be found in this feature.

- The above estimates are robust against variations in assumptions concerning the mass of the LMC central MBH and the MW+LMC gravitational potential ([Fig. 9](#)).

With these results we show that the LMC may be a more bountiful wellspring of HVSs than was previously appreciated. The prospects are promising for current and near-future deep and wide Galactic surveys to increase the population of known HVSs significantly from both the GC and LMC. The confirmation and further study of HVSs can be used as probes to study the structure of the MW and LMC, the interactions between them, and the environments of their MBHs. Our results outline expectations for the number of HVSs we should expect to detect in near-future surveys, provide clues on how to search for these objects effectively and how to offer predictions on how GC HVSs and LMC HVSs will compare and contrast.

ACKNOWLEDGEMENTS

We thank the anonymous referee, whose helpful and considered feedback improved this manuscript. We thank Omar Contigiani and Anthony Brown for helpful discussions. FAE acknowledges funding support from the Natural Sciences and Engineering Research Council of Canada (NSERC) Postgraduate Scholarship. TM acknowledges an ESO fellowship.

DATA AVAILABILITY

The simulation outputs underpinning this work can be shared upon request to the corresponding author.

REFERENCES

- Abadi M. G., Navarro J. F., Steinmetz M., 2009, *ApJ*, **691**, L63
 Anders E., Grevesse N., 1989, *Geochimica Cosmochimica Acta*, **53**, 197
 Bailer-Jones C. A. L., 2015, *PASP*, **127**, 994
 Bartko H., et al., 2010, *ApJ*, **708**, 834
 Bellovary J. M., et al., 2021, arXiv e-prints, p. [arXiv:2102.09566](#)
 Belokurov V., Deason A. J., Erkal D., Koposov S. E., Carballo-Bello J. A., Smith M. C., Jethwa P., Navarrete C., 2019, *MNRAS*, **488**, L47
 Besla G., Kallivayalil N., Hernquist L., Robertson B., Cox T. J., van der Marel R. P., Alcock C., 2007, *ApJ*, **668**, 949
 Bessell M. S., 1990, *PASP*, **102**, 1181
 Blaauw A., 1961, *Bull. Astron. Inst. Netherlands*, **15**, 265
 Bland-Hawthorn J., Gerhard O., 2016, *ARA&A*, **54**, 529
 Böker T., 2010, in de Grijs R., Lépine J. R. D., eds, *IAU Symposium Vol. 266, Star Clusters: Basic Galactic Building Blocks Throughout Time and Space*. pp 58–63 ([arXiv:0910.4863](#)), [doi:10.1017/S1743921309990871](#)
 Boubert D., Evans N. W., 2016, *ApJ*, **825**, L6

- Boubert D., Everall A., 2020, *MNRAS*, **497**, 4246
- Boubert D., Erkal D., Evans N. W., Izzard R. G., 2017, *MNRAS*, **469**, 2151
- Boubert D., Everall A., Holl B., 2020a, *MNRAS*, **497**, 1826
- Boubert D., Erkal D., Gualandris A., 2020b, *MNRAS*, **497**, 2930
- Bovy J., 2015, *ApJS*, **216**, 29
- Bovy J., Rix H.-W., Green G. M., Schlafly E. F., Finkbeiner D. P., 2016, *ApJ*, **818**, 130
- Boyce H., Lützgendorf N., van der Marel R. P., Baumgardt H., Kissler-Patig M., Neumayer N., de Zeeuw P. T., 2017, *ApJ*, **846**, 14
- Bromley B. C., Kenyon S. J., Geller M. J., Brown W. R., 2012, *ApJ*, **749**, L42
- Brown W. R., 2015, *ARA&A*, **53**, 15
- Brown W. R., Geller M. J., Kenyon S. J., Kurtz M. J., 2005, *ApJ*, **622**, L33
- Brown W. R., Geller M. J., Kenyon S. J., Kurtz M. J., 2006, *ApJ*, **640**, L35
- Brown W. R., Geller M. J., Kenyon S. J., Kurtz M. J., Bromley B. C., 2007, *ApJ*, **660**, 311
- Brown W. R., Geller M. J., Kenyon S. J., 2009a, *ApJ*, **690**, 1639
- Brown W. R., Geller M. J., Kenyon S. J., Bromley B. C., 2009b, *ApJ*, **690**, L69
- Brown W. R., Geller M. J., Kenyon S. J., 2012, *ApJ*, **751**, 55
- Brown W. R., Geller M. J., Kenyon S. J., 2014, *ApJ*, **787**, 89
- Cardelli J. A., Clayton G. C., Mathis J. S., 1989, *ApJ*, **345**, 245
- Choudhury S., Subramaniam A., Cole A. A., 2016, *MNRAS*, **455**, 1855
- Contigiani O., Rossi E. M., Marchetti T., 2019, *MNRAS*, **487**, 4025
- Da Rio N., Gouliermis D. A., Henning T., 2009, *ApJ*, **696**, 528
- Do T., Kerzendorf W., Winsor N., Støstad M., Morris M. R., Lu J. R., Ghez A. M., 2015, *ApJ*, **809**, 143
- Dormand J., Prince P., 1980, *Journal of Computational and Applied Mathematics*, **6**, 19
- Drimmel R., Cabrera-Lavers A., López-Corredoira M., 2003, *A&A*, **409**, 205
- Dunstall P. R., et al., 2015, *A&A*, **580**, A93
- Edelmann H., Napiwotzki R., Heber U., Christlieb N., Reimers D., 2005, *ApJ*, **634**, L181
- Eisenhauer F., et al., 2005, *Apj*, **628**, 246
- Erkal D., Belokurov V. A., 2020, *MNRAS*, **495**, 2554
- Erkal D., Boubert D., Gualandris A., Evans N. W., Antonini F., 2019a, *MNRAS*, **483**, 2007
- Erkal D., et al., 2019b, *MNRAS*, **487**, 2685
- Erkal D., Belokurov V. A., Parkin D. L., 2020, *MNRAS*, **498**, 5574
- Evans C. J., et al., 2011, *A&A*, **530**, A108
- Evans F. A., Renzo M., Rossi E. M., 2020, *MNRAS*, **497**, 5344
- Fabricius C., et al., 2021, *A&A*, **649**, A5
- Feldmeier-Krause A., Kerzendorf W., Neumayer N., Schödel R., Noguera-Lara F., Do T., de Zeeuw P. T., Kuntschner H., 2017, *MNRAS*, **464**, 194
- Gaia Collaboration et al., 2016a, *A&A*, **595**, A1
- Gaia Collaboration et al., 2016b, *A&A*, **595**, A2
- Gaia Collaboration et al., 2018, *A&A*, **616**, A1
- Gaia Collaboration et al., 2020, arXiv e-prints, p. arXiv:2012.01771
- Gaia Collaboration et al., 2021, *A&A*, **649**, A1
- Garavito-Camargo N., Besla G., Laporte C. F. P., Johnston K. V., Gómez F. A., Watkins L. L., 2019, *ApJ*, **884**, 51
- Genzel R., Eisenhauer F., Gillessen S., 2010, *Reviews of Modern Physics*, **82**, 3121
- Gezari S., et al., 2009, *ApJ*, **698**, 1367
- Ghez A. M., et al., 2008, *ApJ*, **689**, 1044
- Gnedin O. Y., Gould A., Miralda-Escudé J., Zentner A. R., 2005, *ApJ*, **634**, 344
- Gómez F. A., Besla G., Carpintero D. D., Villalobos Á., O'Shea B. W., Bell E. F., 2015, *ApJ*, **802**, 128
- Green G. M., et al., 2015, *ApJ*, **810**, 25
- Gualandris A., Portegies Zwart S., 2007, *MNRAS*, **376**, L29
- Hattori K., Valluri M., Bell E. F., Roederer I. U., 2018, *ApJ*, **866**, 121
- Heber U., Edelmann H., Napiwotzki R., Altmann M., Scholz R. D., 2008, *A&A*, **483**, L21
- Hernquist L., 1990, *ApJ*, **356**, 359
- Hills J. G., 1988, *Nature*, **331**, 687
- Hirsch H. A., Heber U., O'Toole S. J., Bresolin F., 2005, *A&A*, **444**, L61
- Hobbs D., et al., 2016, arXiv e-prints, p. arXiv:1609.07325
- Huang Y., et al., 2017, *ApJ*, **847**, L9
- Hurley J. R., Pols O. R., Tout C. A., 2000, *MNRAS*, **315**, 543
- Irrgang A., Kreuzer S., Heber U., 2018, *A&A*, **620**, A48
- Irrgang A., Geier S., Heber U., Kupfer T., Fürst F., 2019, *A&A*, **628**, L5
- Ivezic Ž., Beers T. C., Jurić M., 2012, *ARA&A*, **50**, 251
- Ivezic Ž., et al., 2019, *ApJ*, **873**, 111
- Izzard R. G., Glebbeek E., Stancliffe R. J., Pols O. R., 2009, *A&A*, **508**, 1359
- Jordi C., et al., 2010, *A&A*, **523**, A48
- Kallivayalil N., van der Marel R. P., Besla G., Anderson J., Alcock C., 2013, *ApJ*, **764**, 161
- Katz D., et al., 2019, *A&A*, **622**, A205
- Kenyon S. J., Bromley B. C., Geller M. J., Brown W. R., 2008, *ApJ*, **680**, 312
- Kenyon S. J., Bromley B. C., Brown W. R., Geller M. J., 2014, *ApJ*, **793**, 122
- Kenyon S. J., Bromley B. C., Brown W. R., Geller M. J., 2018, *ApJ*, **864**, 130
- Kobayashi S., Hainick Y., Sari R., Rossi E. M., 2012, *ApJ*, **748**, 105
- Koposov S. E., et al., 2020, *MNRAS*, **491**, 2465
- Kreuzer S., Irrgang A., Heber U., 2020, *A&A*, **637**, A53
- Kroupa P., 2001, *MNRAS*, **322**, 231
- LSST Science Collaboration et al., 2017, arXiv e-prints, p. arXiv:1708.04058
- Laporte C. F. P., Gómez F. A., Besla G., Johnston K. V., Garavito-Camargo N., 2018, *MNRAS*, **473**, 1218
- Leonard P. J. T., 1991, *AJ*, **101**, 562
- Leonard P. J. T., Duncan M. J., 1990, *AJ*, **99**, 608
- Li Y.-B., et al., 2018, *AJ*, **156**, 87
- Li T. S., et al., 2019, *MNRAS*, **490**, 3508
- Lindegren L., et al., 2018, *A&A*, **616**, A2
- Lindegren L., et al., 2021, *A&A*, **649**, A2
- Liu Q., de Grijs R., Deng L. C., Hu Y., Baraffe I., Beaulieu S. F., 2009a, *MNRAS*, **396**, 1665
- Liu Q., de Grijs R., Deng L. C., Hu Y., Beaulieu S. F., 2009b, *A&A*, **503**, 469
- Löckmann U., Baumgardt H., Kroupa P., 2010, *MNRAS*, **402**, 519
- Lu Y., Yu Q., Lin D. N. C., 2007, *ApJ*, **666**, L89
- Lu J. R., Do T., Ghez A. M., Morris M. R., Yelda S., Matthews K., 2013, *ApJ*, **764**, 155
- Mackey A. D., Koposov S. E., Erkal D., Belokurov V., Da Costa G. S., Gómez F. A., 2016, *MNRAS*, **459**, 239
- Madigan A.-M., Pfuhl O., Levin Y., Gillessen S., Genzel R., Perets H. B., 2014, *ApJ*, **784**, 23
- Marchetti T., 2021, *MNRAS*, **503**, 1374
- Marchetti T., Rossi E. M., Kordopatis G., Brown A. G. A., Rimoldi A., Starkenburg E., Youakim K., Ashley R., 2017, *MNRAS*, **470**, 1388
- Marchetti T., Contigiani O., Rossi E. M., Albert J. G., Brown A. G. A., Sesana A., 2018, *MNRAS*, **476**, 4697
- Marchetti T., Rossi E. M., Brown A. G. A., 2019, *MNRAS*, **490**, 157
- Marshall D. J., Robin A. C., Reylé C., Schultheis M., Picaud S., 2006, *A&A*, **453**, 635
- McMillan P. J., 2017, *MNRAS*, **465**, 76
- Mezcua M., Domínguez Sánchez H., 2020, *ApJ*, **898**, L30
- Miyamoto M., Nagai R., 1975, *PASJ*, **27**, 533

- Moe M., Stefano R. D., 2013, *ApJ*, 778, 95
- Navarro J. F., Frenk C. S., White S. D. M., 1996, *ApJ*, 462, 563
- Navarro J. F., Frenk C. S., White S. D. M., 1997, *ApJ*, 490, 493
- Oh S., Kroupa P., 2016, *A&A*, 590, A107
- Õpik E., 1924, Publications of the Tartu Astrofizica Observatory, 25, 1
- Palladino L. E., Schlesinger K. J., Holley-Bockelmann K., Allende Prieto C., Beers T. C., Lee Y. S., Schneider D. P., 2014, *ApJ*, 780, 7
- Patel E., Besla G., Sohn S. T., 2017, *MNRAS*, 464, 3825
- Peñarrubia J., Gómez F. A., Besla G., Erkal D., Ma Y.-Z., 2016, *MNRAS*, 456, L54
- Pecaut M. J., Mamajek E. E., 2013, *ApJS*, 208, 9
- Perets H. B., Šubr L., 2012, *ApJ*, 751, 133
- Petersen M. S., Peñarrubia J., 2020, *MNRAS*, 494, L11
- Petts J. A., Read J. I., Gualandris A., 2016, *MNRAS*, 463, 858
- Piatti A. E., Geisler D., 2013, *AJ*, 145, 17
- Pietrzyński G., et al., 2013, *Nature*, 495, 76
- Planck Collaboration et al., 2016, *A&A*, 594, A13
- Portegies Zwart S. F., 2000, *ApJ*, 544, 437
- Poveda A., Ruiz J., Allen C., 1967, Boletín de los Observatorios Tonantzintla y Tacubaya, 4, 86
- Price-Whelan A. M., Hogg D. W., Johnston K. V., Hendel D., 2014, *Apj*, 794, 4
- Przybillá N., Nieva M. F., Heber U., Firnstein M., Butler K., Napiwotzki R., Edelmann H., 2008, *A&A*, 480, L37
- Raddi R., Irrgang A., Heber U., Schneider D., Kreuzer S., 2021, *A&A*, 645, A108
- Reines A. E., Greene J. E., Geha M., 2013, *ApJ*, 775, 116
- Reines A. E., Condon J. J., Darling J., Greene J. E., 2020, *ApJ*, 888, 36
- Renzo M., et al., 2019, *A&A*, 624, A66
- Rich R. M., Ryde N., Thorsbro B., Fritz T. K., Schultheis M., Origlia L., Jönsson H., 2017, *AJ*, 154, 239
- Rossi E. M., Kobayashi S., Sari R., 2014, *ApJ*, 795, 125
- Rossi E. M., Marchetti T., Cacciato M., Kuiack M., Sari R., 2017, *MNRAS*, 467, 1844
- Sari R., Kobayashi S., Rossi E. M., 2010, *ApJ*, 708, 605
- Schönrich R., 2012, *MNRAS*, 427, 274
- Sherwin B. D., Loeb A., O’Leary R. M., 2008, *MNRAS*, 386, 1179
- Silva M. D. V., Napiwotzki R., 2011, *MNRAS*, 411, 2596
- Stone N. C., Metzger B. D., 2016, *MNRAS*, 455, 859
- Tauris T. M., 2015, *MNRAS*, 448, L6
- Tauris T. M., Takens R. J., 1998, *A&A*, 330, 1047
- The GRAVITY Collaboration et al., 2019, *A&A*, 625, L10
- Wang J., Merritt D., 2004, *ApJ*, 600, 149
- Westera P., Lejeune T., Buser R., Cuisinier F., Bruzual G., 2002, *A&A*, 381, 524
- Yu Q., Madau P., 2007, *MNRAS*, 379, 1293
- Yu Q., Tremaine S., 2003, *ApJ*, 599, 1129
- Zhang F., Lu Y., Yu Q., 2013, *ApJ*, 768, 153
- Zhong J., et al., 2014, *ApJ*, 789, L2
- Zivick P., et al., 2019, *ApJ*, 874, 78
- van Velzen S., Farrar G. R., 2014, *ApJ*, 792, 53
- van der Marel R. P., Kallivayalil N., 2014, *ApJ*, 781, 121
- van der Marel R. P., Alves D. R., Hardy E., Suntzeff N. B., 2002, *AJ*, 124, 2639

This paper has been typeset from a $\text{T}_{\text{E}}\text{X}/\text{L}^{\text{A}}\text{T}_{\text{E}}\text{X}$ file prepared by the author.